Toward Reliable Identification of 2D Monolayer vs Multilayer: Optical and AFM Analysis of MoS_2 obtained with CVD and Mechanical Exfoliation methods

by

Batyrkhan Mustafin

A Thesis Submitted to the Faculty of the

DEPARTMENT OF PHYSICS

In Partial Fulfillment of the Requirements

For the Degree of

BACHELOR OF SCIENCE

In the School of Science and Humanities

NAZARBAYEV UNIVERSITY

2025

Abstract

This thesis presents a comprehensive study on the fabrication and reliable identification of monolayer molybdenum disulfide (MoS_2) using two distinct methods: face-to-face chemical vapor deposition (CVD) and mechanical exfoliation. The CVD growth process was based on an established methodology within our research group, and efforts in this work focused on fine-tuning growth parameters and characterization. In parallel, mechanical exfoliation was introduced as a new technique, with this thesis being the first to develop and optimize it within the group for producing monolayer MoS_2. Comprehensive characterization of the resulting flakes from both methods was carried out using atomic force microscopy (AFM), Raman spectroscopy, photoluminescence (PL), and a co-localized approach. One exfoliated flake displayed excellent agreement across all techniques, confirming it as a high-quality monolayer (strong PL at ~1.85 eV, ~16 cm^{-1} Raman mode separation, and ~0.8 nm AFM height). Another flake showed monolayer-like optical features but a significantly larger AFM thickness (~5.5–7.6 nm), highlighting the necessity of multi-modal analysis. The thesis also details the development and verification of a custom mini-probe station for upcoming low-temperature optical and electrical experiments. Although optical access constraints prevented cryogenic PL, the technology was successfully tested using TiN thin films. The findings provide a robust reference for assessing CVD-grown monolayers and contribute to improving both fabrication and verification techniques for 2D materials.

Key Results: Two fabrication routes for monolayer MoS_2 were established and systematically explored: (1) face-to-face CVD growth and (2) mechanical exfoliation. The CVD method, already in use within the group, was optimized through parameter tuning to improve the yield and uniformity of triangular monolayer domains on SiO_2/Si substrates. Optical contrast, Raman spectroscopy, and PL confirmed the monolayer nature of select domains, with Raman mode separations of ~18–20 cm^{-1} and strong PL near 1.85 eV. AFM confirmed ~0.8 nm thickness for these domains. Concurrently, mechanical exfoliation was introduced and developed for the first time in the lab. Using careful sample preparation and substrate handling, exfoliated flakes of varying thicknesses were obtained. One such flake showed full consistency across Raman, PL, and AFM, confirming its monolayer nature. Another exfoliated flake exhibited an unusual discrepancy: monolayer-like optical behavior but an AFM-measured thickness of 5.5–7.6 nm. This anomaly, unresolved in origin, underscores the value of co-localized multi-technique verification. A custom mini-probe station was constructed and successfully tested on TiN thin films, though limitations in optical access prevented cryogenic optical measurements on MoS_2 samples at this stage.

Significance: This work advances both the fabrication and the characterization of monolayer MoS_2. The face-to-face CVD growth approach demonstrates a route to high-quality, large-area monolayer MoS_2, important for scalable 2D electronics. The exfoliated flakes, particularly those with consistent Raman, PL, and AFM data, provide reliable benchmarks for evaluating the quality of CVD-grown samples. The design and testing of the mini-probe station lay the groundwork for future electrical measurements on CVD-grown 2D materials. Collectively, this work strengthens the experimental toolkit for 2D materials research and advances the reliability of monolayer MoS_2 integration into optoelectronic devices.

Introduction

Background and Motivation

Two-dimensional (2D) materials have emerged as a revolutionary class of materials in physics and nanotechnology, offering unique properties distinct from their bulk counterparts [1]. The discovery of graphene in 2004 opened the door to this field, and since then, many other 2D materials beyond graphene have been explored [2]. In particular, transition metal dichalcogenides (TMDs) such as MoS_2 have attracted intense interest for next-generation electronic and photonic applications [1]. Monolayer MoS_2 is a semiconducting TMD that exhibits a direct bandgap of approximately 1.8–1.9 eV, whereas in bulk form MoS_2 has an indirect bandgap of ~1.2 eV. This direct bandgap in the monolayer leads to strong photoluminescence and makes monolayer MoS_2 highly attractive for optoelectronics. Indeed, monolayer MoS_2 was first shown to emit brightly in the visible range due to this direct gap, in contrast to the weak emission from bulk MoS_2. The reduced dimensionality also gives rise to strongly bound excitons (electron–hole pairs) in monolayer MoS_2, which dominate its optical response. Moreover, the combination of broken inversion symmetry and strong spin–orbit coupling in monolayer MoS_2 leads to coupled spin and valley degrees of freedom [3]. This spin–valley coupling enables phenomena such as selective circularly polarized emission and valley polarization, making monolayer MoS_2 interesting for fundamental physics (e.g. valleytronics).

Beyond optical properties, monolayer MoS_2 also shows remarkable electronic behavior. It can support a high on/off ratio field-effect transistors (FETs) because of its finite bandgap, something not achievable with gapless graphene. For example, early experiments demonstrated back-gated monolayer MoS_2 FETs with on/off current ratios exceeding 10^8, suitable for logic applications. These FETs, reported in 2011, confirmed that MoS_2 could be used to make ultrathin transistors with excellent switching behavior. However, the carrier mobility in initially tested MoS_2 monolayers was modest (tens of $cm^2/V \cdot s$) due to substrate interactions and impurities, spurring efforts to improve material quality. Overall, the attractive electronic and optical properties of monolayer MoS_2 position it as a promising material for transistors, photodetectors, light-emitting devices, and other nanoscale applications [1].

Research to date on MoS_2 and other 2D materials has followed two major paths: (1) mechanical exfoliation of bulk crystals, and (2) chemical vapor deposition growth of thin layers. Mechanical exfoliation (the “Scotch tape” method) was famously used to isolate graphene and was soon applied to MoS_2, yielding high-quality monolayer flakes suitable for fundamental studies [2]. Exfoliated monolayers of MoS_2 have been used to reveal its intrinsic properties, such as the direct bandgap and resultant photoluminescence, as well as to fabricate prototype transistors demonstrating the material’s potential. However, exfoliation produces only small, random flakes and is not a scalable technique for large-area device fabrication. To enable practical applications, CVD growth methods have been developed to synthesize monolayer MoS_2 on substrates over large areas [1]. CVD-grown MoS_2 was first reported in

2012, when researchers demonstrated centimeter-scale MoS_2 atomic layers on SiO_2/Si substrates by reacting MoO_3 and sulfur at high temperature. Since then, CVD techniques have achieved improved uniformity and domain size, including epitaxial monolayer films and continuous polycrystalline monolayers on wafers [1]. Despite these advances, challenges remain in reproducing the pristine quality of exfoliated flakes with CVD growth. Issues such as grain boundaries in CVD films (where individual crystalline domains merge) and unintentional defects can affect material properties. Understanding how the synthesis method influences MoS_2's properties is crucial for optimizing its performance in devices.

We aim to develop a CVD growth process that yields monolayer MoS_2 with quality approaching that of exfoliated crystals. Additionally, we seek to measure not just the optical characteristics of these monolayers, but also their electrical behavior – a step necessary to evaluate device performance. This motivated the second major effort of this project: constructing a miniature probe station to electrically probe micro-scale MoS_2 samples and perform PL measurements under low temperature. By integrating growth and characterization we can more comprehensively assess the monolayers' readiness for applications.

However, reliably producing and identifying monolayer MoS_2 remains a practical challenge. Mechanical exfoliation (the "Scotch tape" method) can yield high-quality monolayers, but with limited size and reproducibility. Chemical vapor deposition (CVD) offers a path to scalable synthesis of monolayer MoS_2 over large areas, but optimizing such growth to consistently achieve monolayers is non-trivial. False positives can occur: for instance, flakes might show monolayer-like optical contrast or spectra, yet actually consist of multiple layers or have unforeseen thickness anomalies. Thus, careful characterization using multiple techniques is essential to unequivocally identify a true monolayer and assess its quality. In this work, we address these issues by combining CVD growth attempts with parallel efforts on exfoliated MoS_2, using the latter as a benchmark for monolayer properties. By applying Raman spectroscopy, photoluminescence (PL) spectroscopy, and atomic force microscopy (AFM) to the same flake, we demonstrate a robust identification of a monolayer region and characterize how its properties diverge from few-layer regions of the same flake. This multi-modal approach provides a template for verifying monolayer nature in both exfoliated and CVD-grown samples.

We also touch on the potential of low-temperature (cryogenic) measurements in advancing the characterization of 2D materials. Cryogenic Raman and PL spectroscopy can sharpen spectral features and reveal additional phenomena (such as exciton fine structure or defect-bound states) that are not discernible at room temperature. While the experimental data in this thesis were collected at ambient conditions, we discuss how cryogenic measurements could further enhance the analysis of MoS_2 monolayers, providing higher resolution and deeper insight into their excitonic and vibrational dynamics.

Research Objectives

The objectives of this bachelor's thesis are as follows:

- **CVD Parameter Optimization:** To refine and optimize an existing face-to-face CVD method for MoS_2 growth by adjusting variables such as H_2S flow rate, substrate configuration, and seeding conditions in order to enhance domain size, coverage, and monolayer quality.

- **Exfoliated Monolayer Identification:** To perform detailed, co-localized characterization of exfoliated MoS_2 flakes using Raman spectroscopy, PL, and AFM. The goal is to identify regions with consistent monolayer signatures across all three techniques and establish these as benchmark standards.

- **Analysis of Optical–Topographical Discrepancies:** To investigate and document any inconsistencies in thickness measurements, such as flakes showing monolayer optical behavior but anomalously large AFM heights. This includes exploring plausible physical explanations and assessing the limitations of each technique.

- **Multi-Modal Characterization Methodology:** To demonstrate the value of combining spatially aligned measurements across multiple platforms (AFM, Raman, PL) for verifying monolayer nature and detecting hidden anomalies in 2D materials.

- **Probe Station Development:** To design, assemble, and validate a mini-probe station capable of performing electrical measurements and enabling future cryogenic PL studies. The system is benchmarked using temperature-dependent resistance measurements of a TiN thin film.

By achieving these objectives, the thesis aims to advance the reliable production of MoS_2 monolayers and highlight best practices for their verification. The broader goal is to support the development of 2D material technology by improving synthesis techniques and ensuring that the materials meet the required quality standards for research and applications.

Theoretical Background

Two-Dimensional Transition Metal Dichalcogenides (TMDs)

Layered Structure: Transition metal dichalcogenides are compounds of the form MX_2 (where M is a transition metal such as Mo or W, and X is a chalcogen such as S, Se, or Te) that form layered crystals bonded by van der Waals forces. In the case of MoS_2, the crystal structure is hexagonal and belongs to the 2H phase (trigonal prismatic coordination). Each monolayer of MoS_2 consists of a sandwich-like arrangement: one layer of molybdenum atoms is sandwiched between two layers of sulfur atoms (S–Mo–S), forming a covalently bonded unit about 0.65–0.7 nm thick. Adjacent MoS_2 layers are held together by much weaker van der Waals interactions, meaning the layers can be easily peeled apart or exfoliated. This layered structure is what enables the isolation of single monolayers: mechanical exfoliation can overcome the weak interlayer forces without breaking the strong in-layer bonds. The ability to obtain free-standing monolayers allows researchers to study true two-dimensional sheets of MoS_2 and other TMDs.

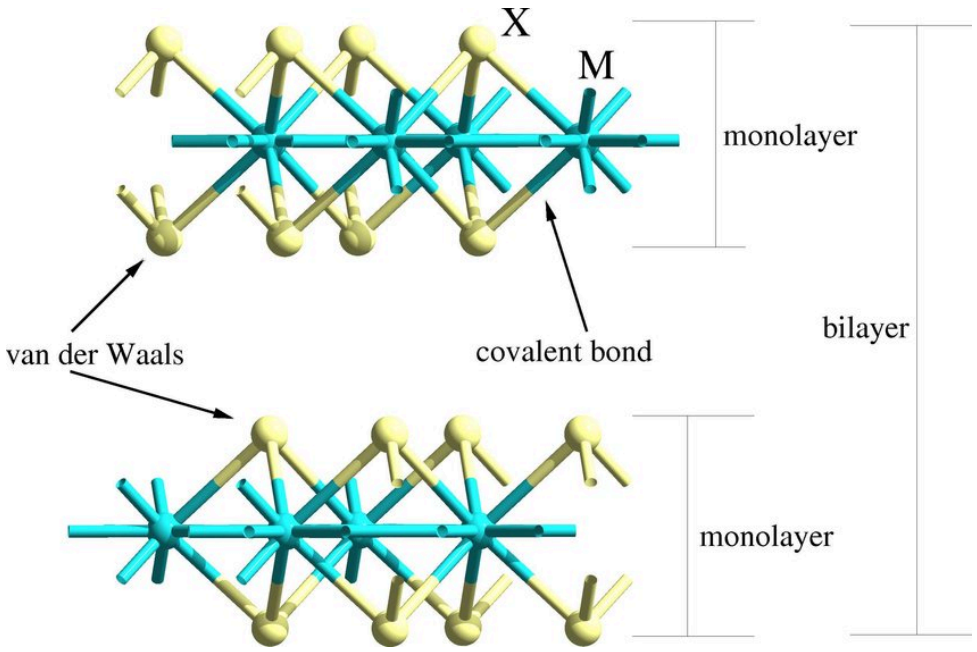

Figure 1. Schematic atomic structure of Transition metal dichalcogenides. [10]

Thickness-Dependent Properties: TMDs exhibit strongly thickness-dependent electronic and optical properties. Many semiconducting TMDs (e.g. MoS_2, WS_2) transition from an indirect bandgap in the bulk to a direct bandgap in the monolayer. For MoS_2, bulk crystals have an indirect bandgap of about 1.2 eV, whereas a single layer has a direct bandgap of ~1.8 eV. As a result, photoluminescence is extremely weak for bulk MoS_2 but becomes very strong for monolayers. This was first demonstrated by Splendiani *et al.* in 2010, who observed the "emerging" PL in monolayer MoS_2 that is absent in few-layer samples [4]. The dramatic increase in PL indicates that electron-hole recombination occurs efficiently in monolayers (direct gap), unlike in bulk, where it is a two-step indirect process. The change in band

structure is accompanied by other layer-dependent effects: for instance, the bandgap energy increases as thickness decreases (a quantum confinement effect), and the exciton binding energy is much larger in monolayers (on the order of 0.5 eV) due to reduced dielectric screening in two dimensions [5]. Additionally, monolayer TMDs have a single layer of atoms, so surface effects and interface interactions can significantly influence their behavior (e.g. adsorbates can dope or quench luminescence).

Unique Physics in Monolayers: Monolayer TMDs like MoS_2 also exhibit unique physics not present in the bulk form. One notable aspect is the strong spin–orbit coupling (SOC) combined with the lack of inversion symmetry in monolayer 2H-MoS_2. Bulk 2H-MoS_2 has inversion symmetry (because it consists of two oppositely oriented monolayers per unit cell), but a single layer is non-centrosymmetric. This leads to a coupling of spin and valley degrees of freedom: electrons in the K and K' valleys (inequivalent corners of the Brillouin zone) have their spins locked to the valley index [3]. In practical terms, this means one can use circularly polarized light to address specific valleys in monolayer MoS_2, creating a valley polarization[3]. Experiments have indeed demonstrated valley-selective circular dichroism in monolayer MoS_2, where right- vs left-circularly polarized excitation preferentially excites one valley or the other [3]. This spin–valley locking is a direct consequence of the broken inversion symmetry and does not occur in the bulk. It has spurred the new subfield of valleytronics, which aims to use the valley index of charge carriers as an information degree of freedom analogous to spin. Furthermore, monolayer MoS_2's strong SOC splits the valence band by hundreds of meV, giving rise to two excitonic transitions (labeled A and B excitons, with B being at higher energy ~2.0 eV due to the spin-split band). These rich physical phenomena make monolayer MoS_2 a fertile platform for exploring low-dimensional quantum physics and developing novel devices.

Raman Spectroscopy of Layered MoS_2

Raman spectroscopy is a powerful, non-destructive tool for probing vibrational modes in materials. In MoS_2 (2H phase), the two prominent first-order Raman-active modes are the in-plane E_2g^1 mode (often denoted E′ for monolayer symmetry) and the out-of-plane A_1g mode (denoted A'_1 in monolayer). In bulk 2H-MoS_2, these modes appear at approximately ~382 cm^{-1} (E_2g^1) and ~408 cm^{-1} (A_1g) [6]. As the thickness is reduced to a single layer, the frequencies of these modes shift due to the absence of interlayer interactions: the in-plane mode softens (red-shifts to lower frequency) and the out-of-plane mode stiffens (blue-shifts) relative to the bulk [6]. In monolayer MoS_2, the E′ mode is typically observed around ~384–385 cm^{-1} and the A'_1 mode around ~403–405 cm^{-1}[6]. The frequency difference between these two peaks ($\Delta = A_1g - E_2g$) is a convenient indicator of layer number. In bulk MoS_2, Δ is on the order of ~25 cm^{-1}, whereas in a monolayer it narrows to ~19–20 cm^{-1} [7]. Bilayer MoS_2 shows an intermediate behavior, with Δ typically in the ~21–22 cm^{-1} range [7]. This trend arises because adding layers increases interlayer van der Waals forces that selectively influence the vibrational modes: the E_2g^1 mode (in-plane motion) is affected by interlayer coupling (causing it to shift to lower frequency in thicker samples), while the A_1g mode (out-of-plane sulfur atom vibration) is constrained by the presence of adjacent layers

(causing it to shift to higher frequency with additional layers) [7]. Thus, by measuring the Raman spectrum of an MoS_2 flake, one can deduce its thickness: a monolayer is confirmed by a small E–A peak separation (~19 cm^{-1}) [7] and specific absolute peak positions, whereas a few-layer or bulk sample will show larger separation and slightly shifted peak frequencies.

In addition to peak positions, the intensity of Raman modes can also depend on layer thickness. Monolayer MoS_2 often exhibits relatively strong Raman signals for both E′ and A'_1 modes (owing to resonance effects with the bandgap), and as layers increase, the overall Raman signal can increase due to the larger volume of material probed. However, interference effects in the layered system and the optical absorption of the material can lead to non-linear scaling of intensity with layer number [8]. Up to a certain number of layers (e.g. 3–4 layers), Raman intensities might increase, but for thicker films, signal absorption or screening can saturate the intensity. In practice, the peak frequency shifts are a more reliable fingerprint of thickness than absolute intensity, since intensity can also be affected by laser focus, sample orientation, and substrate effects. No additional Raman peaks appear for monolayer vs. bulk in the pristine 2H phase. Therefore, our use of Raman spectroscopy focuses on the E′ and A'_1 peak positions and their separation as a diagnostic for monolayer MoS_2.

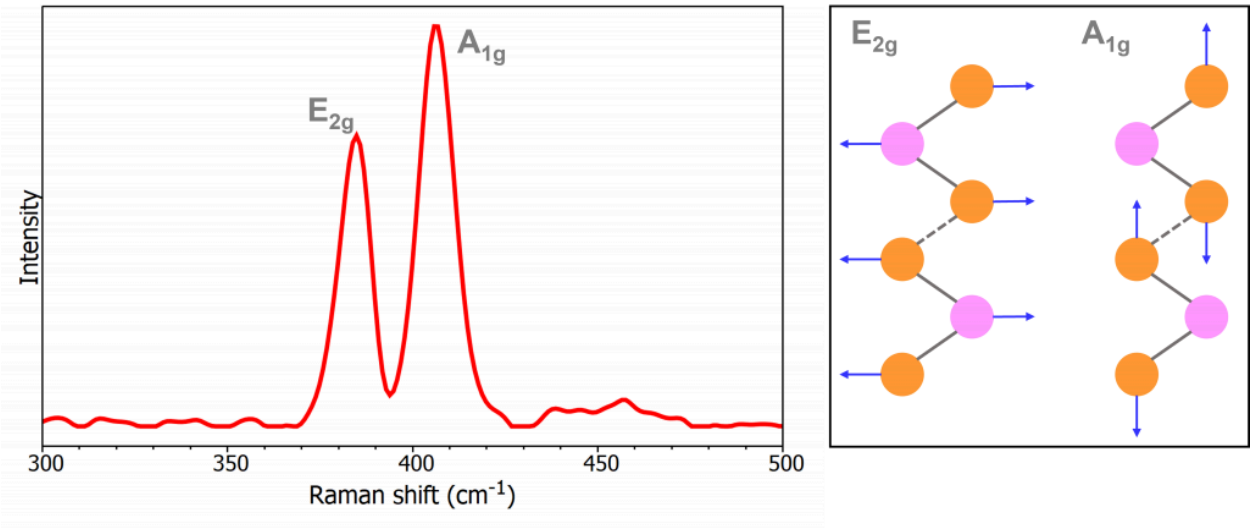

Figure 2. Schematic MoS_2 Raman spectrum (left); E_{2g} and A_{1g} bands vibrations (right). [10]

Photoluminescence in Monolayer vs. Multilayer MoS_2

Monolayer MoS_2 is a direct bandgap semiconductor, and as such it exhibits strong photoluminescence arising from recombination of photoexcited electron–hole pairs (excitons) at the band extrema. The dominant PL feature in monolayer MoS_2 at room temperature is the so-called A exciton emission, appearing around 1.8–1.9 eV (~670–690 nm). A second, higher-energy excitonic transition (the B exciton, ~2.0–2.1 eV) stems from the split valence band (due to spin–orbit coupling) but is typically weaker in PL at room temperature. In contrast, bulk MoS_2 has an indirect bandgap (~1.2 eV) and therefore emits very weakly in

PL; any emission in bulk or multilayer MoS_2 is usually orders of magnitude weaker and often originates from defect or indirect recombination pathways. This direct-to-indirect bandgap crossover occurs already when going from monolayer to bilayer: bilayer MoS_2's fundamental bandgap becomes indirect (the conduction band minimum shifts to a different k-vector), with an energy of roughly ~1.6 eV [8]. As a result, the PL intensity drops dramatically from monolayer to bilayer – monolayer PL can be 10–20× more intense than bilayer under the same excitation. Experiments have shown a "quantum yield" for PL that is highest in monolayers and then plummets for 2 layers and above. For example, Splendiani *et al.* first reported that monolayer MoS_2 shows a bright PL peak near 1.83 eV, whereas the PL from bilayer MoS_2 is much weaker [8]. In some cases, bilayer or trilayer MoS_2 can exhibit a faint, lower-energy emission peak (~1.3–1.5 eV) corresponding to an indirect bandgap transition, but at room temperature this indirect emission is typically very weak. Generally, as thickness increases beyond one layer, the direct exciton emission (at ~1.8 eV) persists but with reduced intensity, and additional red-shifted features may appear due to indirect recombination or defect-bound states, especially in thicker films.

The PL peak energy of the monolayer A exciton can also shift slightly with layer number and environment. In isolated high-quality monolayers on inert substrates, the A exciton is around 1.90 eV at room temperature [8]. On SiO_2/Si substrates (as used in this work), moderate substrate interaction and trapped charges often result in a slight red-shift (e.g. ~1.85 eV observed here, consistent with literature). The linewidth of the PL is another indicator of quality: a narrow PL peak (30–60 meV width at room temperature) suggests good crystalline quality and low disorder. In thicker MoS_2, any direct-gap PL peak (A exciton) is broader and weaker, and the overall emission might be dominated by defect-related broad bands at lower energies. For our purposes, a strong, sharp PL peak near 1.85 eV, with no secondary peaks of comparable intensity, is a clear signature of a monolayer region. Meanwhile, a much lower intensity or multiple broadened peaks would suggest few-layer or bulk material.

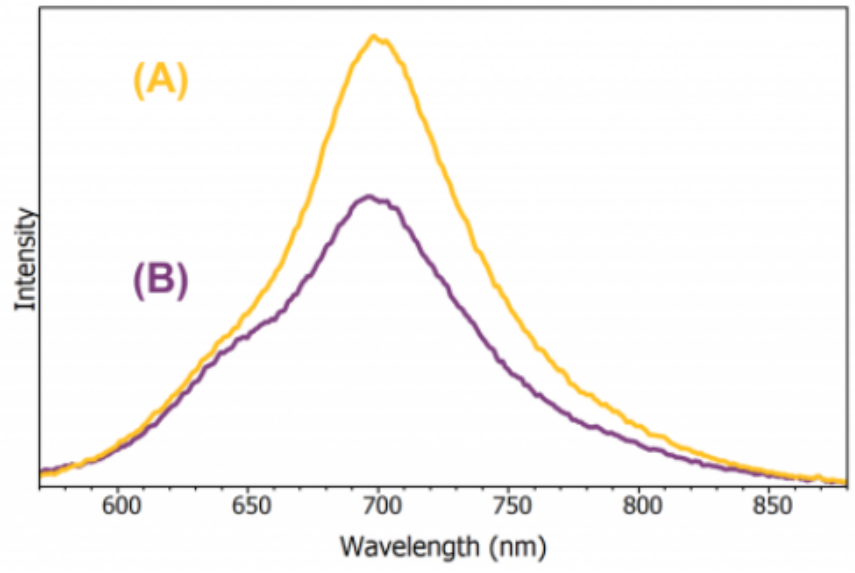

Figure 3. Schematic MoS_2 PL spectrum for a monolayer (A) and multilayer (B). [10]

Utility of Cryogenic Raman and PL Spectroscopy

Performing Raman and PL measurements at cryogenic temperatures (e.g. 10–100 K) can significantly enhance spectral resolution and reveal additional physical effects in MoS_2 and other TMDs. At lower temperatures, phonon populations are reduced and lattice vibrations are less thermally perturbed, leading to narrower Raman linewidths and minor shifts to higher frequencies (due to thermal contraction of the lattice). This can allow closely spaced modes to be distinguished more clearly. For example, the small frequency difference between the E′ and A'_1 modes in few-layer MoS_2 can be measured with higher precision at low temperature, and any subtle splittings of modes (such as interlayer vibrational mode splitting in trilayers) become more discernible with reduced broadening. Low-temperature Raman spectroscopy also enables the study of temperature dependence of phonon frequencies, which can shed light on anharmonic effects and interlayer interactions [7] (often, one observes a slight increase in the E_2g^1–A_1g separation as temperature decreases).

Cryogenic PL spectroscopy is particularly valuable for investigating the excitonic properties of monolayer MoS_2. At 77 K (liquid nitrogen temperature) or even 4 K (liquid helium temperature), the thermal broadening of exciton lines is greatly reduced, resulting in much sharper PL peaks. This improved resolution can reveal features that are washed out at room temperature. In monolayer MoS_2, two notable additional features become evident at low T: the charged exciton (trion) and defect-bound excitons. The trion is a bound state of two electrons and one hole (or two holes and one electron) and in MoS_2 it appears as a peak a few tens of meV below the neutral A exciton. At room temperature, the A exciton and trion peaks often merge into one broad feature (especially if doping is moderate), but at low temperatures they separate into distinct peaks [10]. This allows precise determination of the trion binding energy and fraction [11]. Additionally, low T PL can uncover the B exciton emission (~2.0 eV) which might be weak at room T but becomes more pronounced when thermal population of the higher-energy state is reduced. Moreover, defect-bound excitons (often labeled as D peaks) tend to emerge at energies red-shifted (~0.1–0.2 eV below A) at low temperatures [10]. These are excitons trapped at impurity or vacancy sites and are generally only resolvable when the broadening is small. Identifying such defect-related peaks is important for assessing material quality, as their presence indicates impurities or vacancies.

In summary, cryogenic measurements enhance the detection of multiple excitonic species in monolayer MoS_2 – neutral excitons, trions, bound excitons – and provide cleaner Raman spectra. While our current study was conducted at room temperature (due to equipment limitations, as low-temperature integration was not available), future experiments on the CVD-grown and exfoliated monolayers could greatly benefit from cryogenic PL/Raman. Such measurements could confirm the absence of unexpected peaks (ensuring the flakes are high quality) or could reveal subtle differences between CVD and exfoliated material (for instance, differing defect densities might be reflected in the prominence of bound exciton peaks at low T). The ability to perform low-T spectroscopy will thus be a valuable extension of the characterization toolkit for MoS_2 moving forward.

Applications and Significance: The distinctive properties of monolayer MoS_2 and related TMDs make them promising for a variety of applications. In electronics, monolayer MoS_2 has a sufficiently large bandgap to be used as a channel in field-effect transistors (unlike graphene, which must be engineered to open a gap). Although early devices had modest mobilities, research has shown that with high-κ dielectric environments and better contacts, mobilities can reach >100 $cm^2/V \cdot s$ for monolayer MoS_2 at room temperature. The on/off ratios exceeding 10^8 indicate excellent switching capabilities, which is attractive for low-power logic. In optoelectronics, monolayer MoS_2's direct gap and strong light–matter interaction yield high photoresponsivity in photodetectors [1] and make it a candidate for light-emitting diodes and lasers at visible wavelengths. The strong PL and absorption also enable MoS_2 monolayers to be used in sensing and nonlinear optical applications (for example, saturable absorption in ultrathin optical devices). Additionally, the flexibility and transparency of 2D materials mean they can be integrated onto flexible substrates or stacked into transparent electronics. MoS_2, being just three atoms thick, is almost completely transparent to visible light except at the resonant exciton wavelengths. This could allow stacking monolayer MoS_2 in optically transparent circuits or as part of heterostructures with graphene (which could serve as transparent electrodes).

In summary, the theoretical background of MoS_2 highlights why the monolayer form is so special. The challenge addressed in this thesis is to experimentally realize high-quality monolayer MoS_2 (via CVD growth) and to verify its monolayer nature and properties through rigorous characterization. The next sections describe the methods we employed for synthesis and characterization, followed by the experimental results and an analysis of what they reveal about monolayer MoS_2.

Experimental Methods

Synthesis of MoS_2 Monolayers via Face-to-Face CVD

CVD Setup: Monolayer MoS_2 was grown using a two-zone horizontal tube furnace in a face-to-face CVD configuration.

In this setup, the metal precursor (providing Mo) and the substrate are placed in close proximity facing each other, to create a confined reaction space. Specifically, a SiO_2/Si wafer substrate (50 nm oxide) was placed face-down directly above a solid MoO_3 source during growth. The MoO_3 source was a thin film of MoO_3 on a SiO_2/Si piece, positioned in the center of the furnace's hot zone. A sulfur precursor was introduced in gaseous form. In our growths, sulfur was supplied by a flow of H_2S gas (diluted in argon), which eliminates the need for sublimating solid sulfur and allows precise control of sulfur delivery [5]. During the growth, H_2S (mixed with a carrier gas such as Ar) was flowed through the tube so that sulfur-bearing gas reached the hot zone where the MoO_3 and substrate were located. The face-to-face geometry meant the substrate was only a few millimeters above the MoO_3 source, creating a locally high concentration of reactants in that small gap. This confined

micro-environment promotes efficient reaction of Mo and S and nucleation of MoS_2 on the substrate before the gases are swept away.

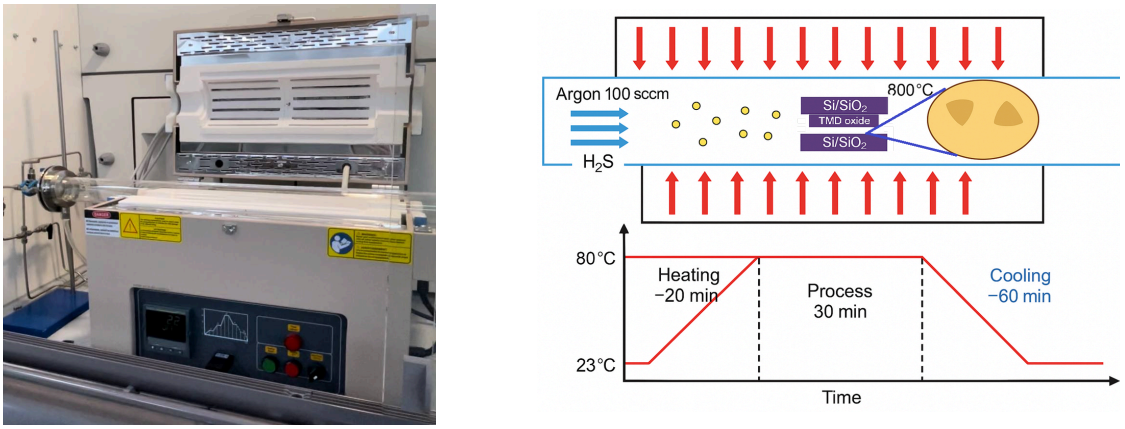

Figure 4. Schematics of the CVD Setup.

Growth Conditions: The temperature and gas flow profile were optimized for MoS_2 monolayer formation. The MoO_3 source and the substrate (which were adjacent) were heated to approximately 800-850 °C. This temperature is sufficient to reduce/evaporate MoO_3 and initiate the reaction with sulfur. The H_2S/Ar gas was introduced once the hot zone reached the target temperature. H_2S is already a gas at room temperature, so its delivery mainly depends on flow control via mass flow controllers. Typical H_2S and Ar total flow rates are approximately 20 sccm (standard cubic centimeters per minute). The growth pressure was ambient or slightly reduced (atmospheric-pressure CVD was used in our case). We included a small flow of hydrogen (H_2) along with H_2S/Ar in some experiments, as H_2 can act as a reducing agent to assist the conversion of MoO_3 to MoS_2 and to improve domain crystallinity. The growth time (the duration of H_2S exposure at high temperature) was around 20-30 minutes. After the growth period, the furnace was allowed to cool naturally while maintaining argon flow to prevent oxidation. Upon cooling to room temperature, the substrates often exhibited a faint yellow, purple, or blue sheen, indicative of MoS_2 layers.

Role of Face-to-Face Geometry: The face-to-face CVD arrangement is known to improve the uniformity of monolayer growth compared to more open configurations [1]. By confining the space between the substrate and the MoO_3 source, the local vapor pressure of Mo and S is increased, leading to more uniform nucleation across the substrate and larger domain sizes. In our experiments, this geometry indeed yielded a few layer MoS_2 domains. These domains typically appeared as triangular single crystals (reflecting MoS_2's hexagonal lattice structure and favored growth directions). In some cases, truncated triangles or hexagonal shapes were observed, depending on growth conditions and relative edge terminations. The high supersaturation in the confined space helps in achieving full monolayer coverage locally, and when multiple nuclei coalesce, a continuous film can form. We also note that using H_2S gas as the sulfur source provided a more consistent and controllable sulfur supply compared to

evaporating solid sulfur. Prior studies have shown that H_2S can lead to well-oriented MoS_2 domains and more reproducible growth [5]. Dumcenco *et al.* reported that H_2S allows control over domain orientation (vertical vs horizontal growth) by tuning the H_2S/H_2 ratio [5], and that large-area continuous films of monolayer MoS_2 could be achieved. In our setup, we introduced small droplets of perylene-3,4,9,10-tetracarboxylic acid (PTAS) to promote nucleation. The presence of such nucleation seeds can increase the density of MoS_2 domains. Most of our growths yielded a high density of triangular monolayer flakes on the substrate, especially in regions with optimal gas flow and temperature.

After growth, the samples were handled carefully to avoid contamination. The substrates with MoS_2 were removed from the furnace and stored in clean containers. We used optical microscopy as an initial check: under 50× magnification, the MoS_2 domains could be seen as tiny triangles with a slight color contrast on the SiO_2 (due to thin-film interference). No chemical etching or transfer was performed; the films were analyzed as-grown on their original substrate.

Preparation of Exfoliated MoS_2 Samples

Mechanical Exfoliation: To obtain pristine monolayer MoS_2 for reference, we used mechanical exfoliation of bulk MoS_2 crystals. High-quality natural MoS_2 crystals were used as the source. A piece of MoS_2 was gently pressed onto a strip of adhesive tape, and the tape was folded and peeled apart to thin out the flakes (the standard Scotch tape method introduced for graphene exfoliation). After such a cleaving step, the tape was likely to have some very thin flakes attached. The tape was then gently pressed onto a clean SiO_2/Si substrate (with 100 nm SiO_2, which is a common thickness that optimizes the optical visibility of monolayer flakes by interference contrast). We used a slow peel technique: the tape was peeled off the substrate very slowly (using a motorized linear stage in some cases) to encourage thin flakes to remain on the substrate. This process left an assortment of MoS_2 flakes of various thicknesses on the SiO_2 surface.

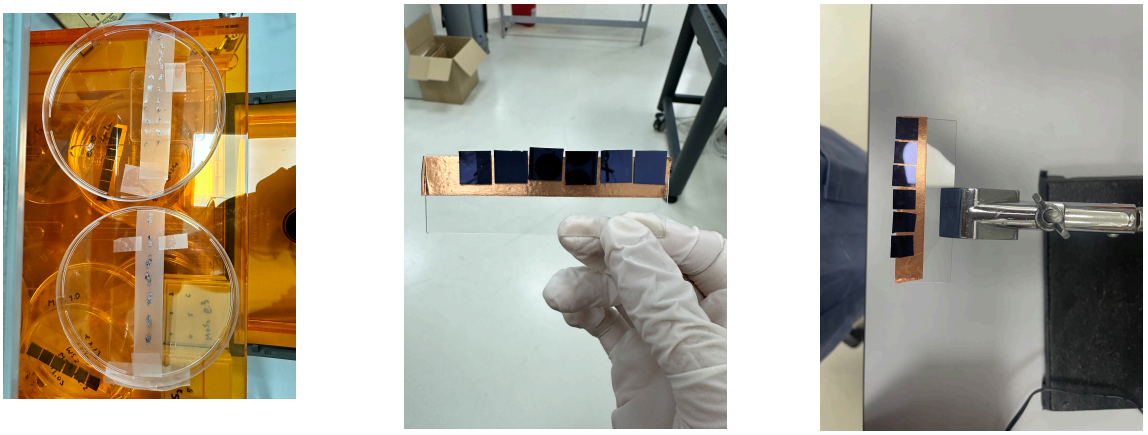

Figure 5. Mother tape as the scotch tape for exfoliated MoS2 (left). Cleaned substrates of SiO2 on the copper tape (mid). Fixed samples using a special adjustable stand (right).

Identifying Monolayers: After exfoliation, we examined the substrate under an optical microscope to locate monolayer candidates. Monolayer MoS_2 on 100 nm SiO_2 is only faintly visible: it typically appears as an extremely light blue or green-purple tint, with very low contrast against the substrate. Thicker flakes (few-layer or bulk) appear with higher contrast (darker colors or visible edges). We searched for flakes that were nearly transparent, visible only due to a slight color hue. One particular flake was identified that had a relatively large area (~10–15 μm across) and was barely discernible in the microscope, suggesting it was either a monolayer or a bilayer. To verify its thickness, we performed quick preliminary Raman and PL checks on this flake: even without a full mapping, a strong PL signal was observed, and a Raman spectrum showed the characteristic ~20 cm^{-1} mode separation. These quick checks indicated the flake's region was monolayer MoS_2. We selected this flake as our primary exfoliated monolayer sample for detailed study.

Raman Spectroscopy

Instrumentation: Raman spectroscopy was carried out using a 532 nm laser as the excitation source. The laser was focused onto the sample by a 100× objective, yielding a spot size of roughly 2 μm. The scattered light was collected by the same objective (back-scattered geometry) and sent through a spectrometer onto a CCD detector. The spectrometer was calibrated using a silicon reference (the Si optical phonon at 520.7 cm^{-1}) to ensure accurate Raman shift measurements. The spectral resolution was on the order of 1 cm^{-1}. Measurements were done in ambient conditions. Laser power was kept low to avoid heating or damaging the monolayers.

Procedure: For the CVD-grown MoS_2, we performed Raman spectra at a few representative spots on the substrate. We specifically targeted visually identified flakes (triangular domains). By focusing on the center of a triangular domain, we could measure Raman peaks that indicate if it is a monolayer. We expected two prominent MoS_2 peaks: the in-plane E_2g^1 (often denoted E') and the out-of-plane A_1g (denoted A'_1 in monolayer). In bulk MoS_2 these occur at roughly 382 cm^{-1} and 408 cm^{-1} respectively. In monolayers, the E' mode shifts up to ~385 cm^{-1} and the A'_1 mode down to ~403 cm^{-1}. Thus, a ~18–20 cm^{-1} separation is a fingerprint of monolayer MoS_2. Our spot measurements on large CVD flakes indeed showed two peaks around 382 and 403 cm^{-1}, with a separation close to 20 cm^{-1}, confirming monolayer features. (We present detailed results in the next section.)

For the exfoliated flakes we have also performed co-localized techniqueas as the flake had varying thickness and that would be useful to see how Raman spectra changes with thickness.

Photoluminescence (PL) Spectroscopy

Instrumentation: PL measurements were performed with the same micro-optical setup as the Raman (using the 532 nm laser for excitation). To measure PL, the spectrometer was configured for a broader spectral range (~550–800 nm) and long integration times. The CCD was calibrated in wavelength (using known emission lines of a calibration lamp). All PL

measurements reported were done at room temperature, as low-temperature PL was not possible due to the microscope working distance issue mentioned earlier.

Procedure: We have performed PL measurements right after Raman at the same spots. We found that even a quick intensity map at ~670 nm (the expected A exciton wavelength for monolayer MoS_2) was very revealing: it showed a bright region corresponding to the flake. For key points (center of flake, edge of flake, off-flake background), we recorded full spectra to check the exact emission energy and spectral shape. For the CVD samples, we collected PL spectra from a few monolayer domains. We have also conducted co-localized measurements on the exfoliated flakes.

Safety and Calibration: As with Raman, laser power was kept low to avoid heating. MoS_2 PL can diminish (thermal quenching) if the flake is overheated by the laser. The spectral calibration was cross-checked by verifying the Si Raman peak position (which can appear in the PL spectrum range if the Raman spectrometer grating is not too low). The PL intensity in counts is relative, but when comparing regions on the same sample, it is meaningful.

Atomic Force Microscopy (AFM)

Setup: AFM measurements were done using a tapping-mode atomic force microscope . In tapping mode, a cantilever with a sharp tip oscillates near its resonance frequency and lightly "taps" the surface. The feedback loop maintains constant oscillation amplitude by adjusting the tip-sample separation, thereby mapping the topography. The exfoliated MoS_2 sample was mounted on the AFM stage, and an optical microscope integrated in the AFM was used to locate the flake. We aligned the AFM scan area to cover the flake's region of interest (approximately 15 μm × 40 μm scan size). The height data were captured with a vertical resolution on the order of angstroms.

Scanning and Data Processing: We scanned the flake in multiple regions. The raw height images were flattened (plane-fit) to remove any tilt of the sample so that the substrate away from the flake could be set as the zero height reference. Key measurements were the step height at the flake's edge relative to the substrate. We measured cross-sectional profiles across the flake to determine its thickness. To ensure the reading was consistent, we performed scans in different areas and directions. No obvious contaminants (like large particles) were seen on top of the flake in the AFM images, which were mostly smooth except at flake edges.

Resolution and Limitations: Our AFM can reliably measure step heights down to a few angstroms, so detecting a ~0.7 nm monolayer step is well within its capability. However, AFM measures the distance to the top of any adsorbed layers or contaminants, so if a water layer or polymer residue exists under or on the flake, the measured "thickness" can be larger than the actual MoS_2 layer itself. We kept this in mind when interpreting results.

With the methods established for growth, exfoliation, optical spectroscopy, and AFM, we proceeded to produce and analyze MoS_2 monolayers. The following section (Results and

Analysis) presents the outcomes of the CVD growth experiments, the performance of the probe station, and the detailed characterization of the exfoliated monolayer flake, along with analysis and discussion of any discrepancies observed.

Mini-Probe Station for Electrical Measurements

Design and Components: A mini-probe station (Instec HCP421V-PM and custom modifications) was constructed to allow electrical probing of microscale samples. The station consists of a stable metal base with a sample stage and four micromanipulator arms holding sharp probe tips. The probe tips are tungsten needles sharpened to <5 μm tip radius, capable of making contact with small pads or flakes. The probe station is connected to a source-measure unit (SMU), Keithley 2450, for electrical measurements. The SMU can source a voltage and measure current (for I–V sweeps) or vice versa.

Figure 6. Mini probe station Instec HCP421V-PM. [11]

Calibration/Test with TiN Sample: Before attempting delicate measurements on MoS_2 monolayers, we tested the probe station using a robust, well-characterized reference material. We used an intrinsic silicon wafer (resistivity ~10 kΩ·cm) uniformly coated with a thin film of titanium nitride (TiN). While TiN is highly conductive and commonly used as a diffusion barrier and electrode material, its electronic nature remains under debate in the literature—variously described as a semiconductor or a semimetal, depending on synthesis and stoichiometry.

To verify the electrical performance of the measurement system, we conducted four-probe resistance measurements by placing probes along the TiN surface, with evenly spaced contacts. We recorded the resistance as a function of temperature from –100 °C to 200 °C. The measured resistance showed a monotonic decrease with increasing temperature, consistent with semiconducting or semi-metallic behavior, where thermally activated carriers or changes in scattering mechanisms dominate.

This test demonstrated that:

- Mechanically, the micromanipulators could place the probes reliably on a flat, conductive surface.

- Electrically, the full system—source/measurement unit (SMU), cabling, and probe contacts—was operational, producing clean, reproducible data with low noise.

The TiN test thus verified that the probe station was ready for accurate resistance measurements on temperature-sensitive 2D materials.

Low-Temperature PL Integration (Challenge): The probe station was designed not only for electrical probing but also to integrate with heating and cooling elements for low and high-temperature measurements (e.g., low-T photoluminescence or electroluminescence). However, we encountered a significant challenge: the objective on our spectrometer had a short working distance, meaning the mini probe station with an optical window could not be fitted between the stage and the lens. In practical terms, we could not focus the PL microscope on the MoS_2 flake when the probe station was present. This prevented us from performing low-temperature PL or Raman on a sample – a limitation that was only discovered after setting up the hardware. The solution would be to use a long-working-distance objective, which we did not have in time for this project. As a result, we had to pivot our approach: we postponed combined low-T electrical/optical measurements and instead focused on performing the optical spectroscopy and AFM on the monolayer flake without electrical contacts. The electrical characterization of MoS_2 monolayers remains as future work once the optical setup is upgraded. This experience highlighted an important practical constraint in instrument design: space for optical access is crucial when integrating probe stations with microscopes.

Results and Analysis

MoS_2 Monolayer CVD Growth – Morphology and Optical Characteristics

After performing the face-to-face CVD growths, the SiO_2/Si substrates were examined under an optical microscope and by Raman/PL spectroscopy to evaluate the results. We observed that the deposition produced numerous MoS_2 domains scattered across the substrate. Under 100× optical magnification, these domains appeared as tiny, flat triangular flakes with lateral dimensions up to ~20–30 μm. They showed a slight purple or blue hue on the 100 nm SiO_2, which is consistent with the optical contrast expected of a monolayer (thicker multilayer flakes would exhibit a more visible contrast and different color). The triangles were generally oriented randomly relative to each other, although some local alignment was noticed (possibly due to nucleation facets or slight substrate steps). In areas near where a droplet of PTAS seeding promoter had been placed, the density of flakes was much higher, suggesting that the seeding effectively increased nucleation sites. In some regions, the triangular domains had grown large enough to touch and merge, forming a contiguous polycrystalline

patch. At those merge lines, one can expect grain boundaries, but within each triangular domain, the crystal is a single grain.

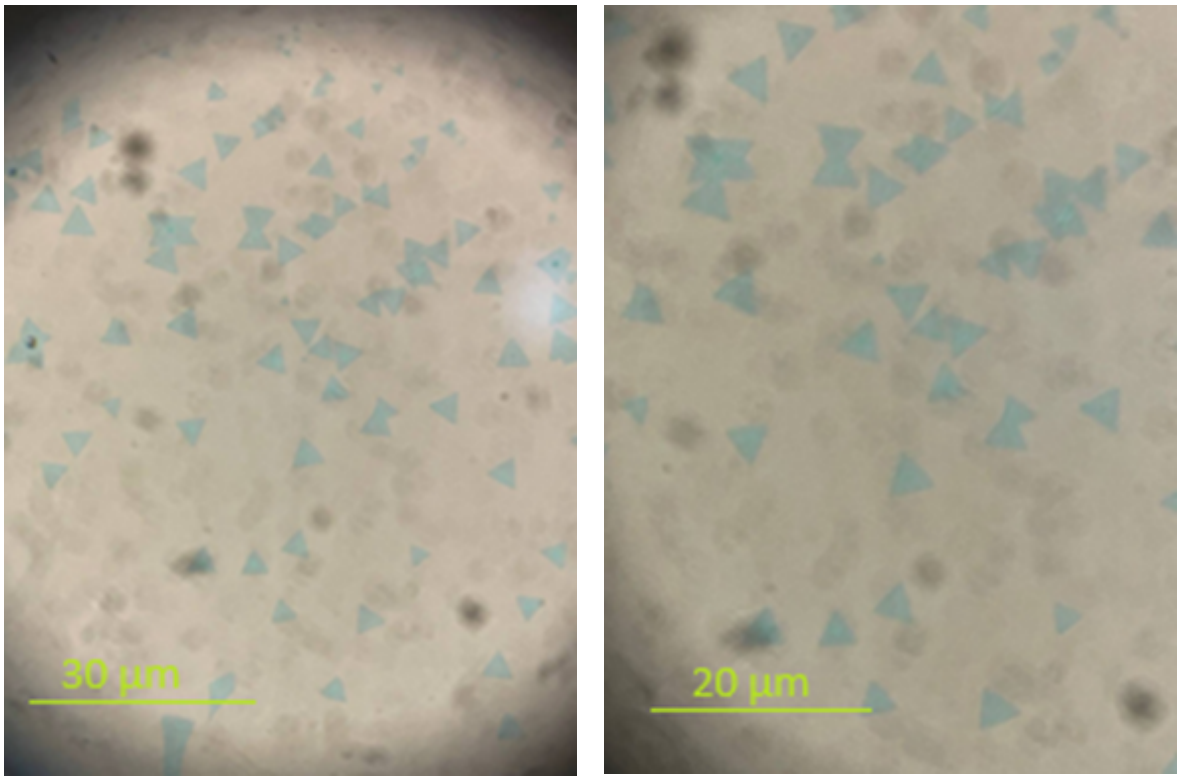

Figure 7. Optical images of the grown MoS_2 flakes.

To verify a few layer nature of these CVD-grown flakes, we collected Raman and PL spectra on representative domains. A typical Raman spectrum from one of the larger triangular flakes showed two prominent peaks around 382 cm^{-1} and 403 cm^{-1}, corresponding to the E' (in-plane) and A'_1 (out-of-plane) vibrational modes of MoS_2 (Figure 1). The separation between these peaks was ~21 cm^{-1}, which falls in the range expected for monolayer MoS_2. Another flake showed a separation of ~20.5 cm^{-1}, also in the monolayer range. These values are significantly smaller than the ~25 cm^{-1} spacing typical of bulk MoS_2, confirming that the CVD flakes are monolayers. The absolute peak positions (e.g., 386 vs 384 cm^{-1}) can vary a couple of wavenumbers depending on strain and doping, but all observed flakes had positions close to literature values for relaxed monolayers. The intensities of the Raman peaks were strong, given the monolayer thickness (and scaled roughly with laser power and focusing), indicating that the MoS_2 is well-coupled to the substrate (a poorly coupled or floating film might have lower Raman intensity).

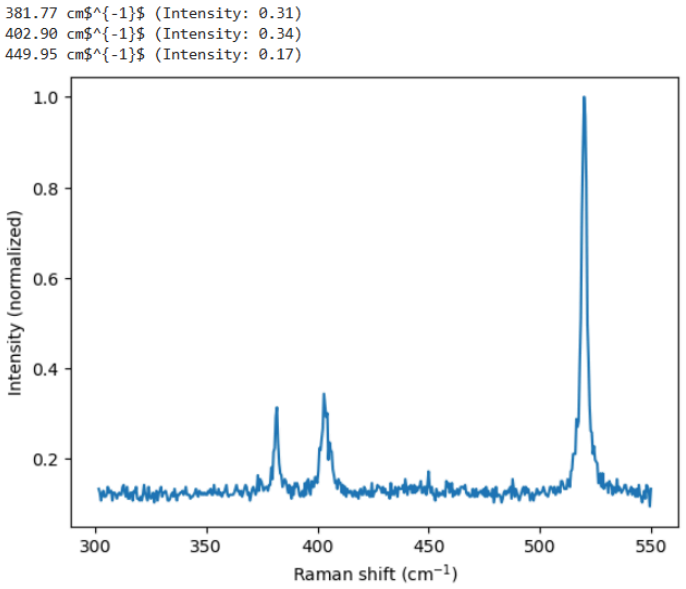

Figure 8. Raman spectra of a CVD grown MoS_2 flake.

Photoluminescence measurements (Figure 9) on the same flakes reinforced the monolayer identification. The PL spectra showed a single dominant emission peak near 1.8 eV (~687 nm). This corresponds to the A exciton recombination in monolayer MoS_2. No low-energy shoulder (which would indicate the indirect bandgap emission of a bilayer or bulk) was present. The bright PL is a hallmark of monolayer MoS_2's direct bandgap; by contrast, a thick multilayer would show quenched PL. We note that the PL peak energies among the flakes were around 1.80–1.85 eV, a small variation possibly due to strain or substrate effects. The fact that these values are close to the exfoliated reference (as we will see) suggests low tensile strain (which would red-shift the PL). The CVD monolayers thus appear to be of good optical quality, emitting nearly as strongly as exfoliated monolayers.

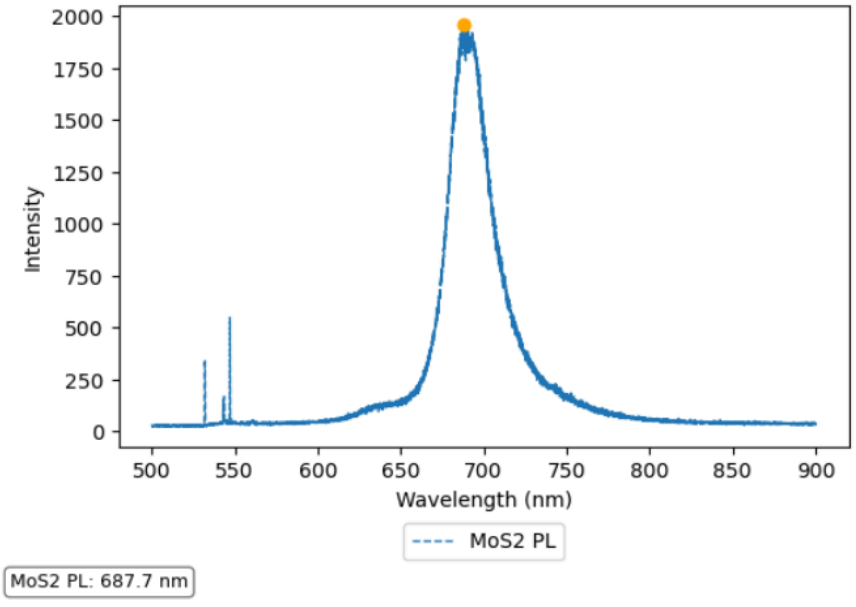

Figure 9. PL spectra of a CVD grown MoS_2 flake.

Finally, we used AFM to measure the thickness of a few CVD MoS_2 domains. On an isolated triangular flake (Figure 10), the AFM height step at the edge was about 2-3 nm, which is inconsistent with a single MoS_2 layer lying on SiO_2. Typical value would be around 0.8 nm for a monolayer. Although, Ramand and PL spectra hint towards a monolayer nature, AFM gives a different result, suggesting 3-4 layer thickness. We did not observe multiple steps or terraces on these triangles, indicating they were uniform regions. AFM scans over merged regions showed some thicker patches at grain boundaries (perhaps small overlaps or second-layer nuclei), but the majority of the area was at monolayer height.

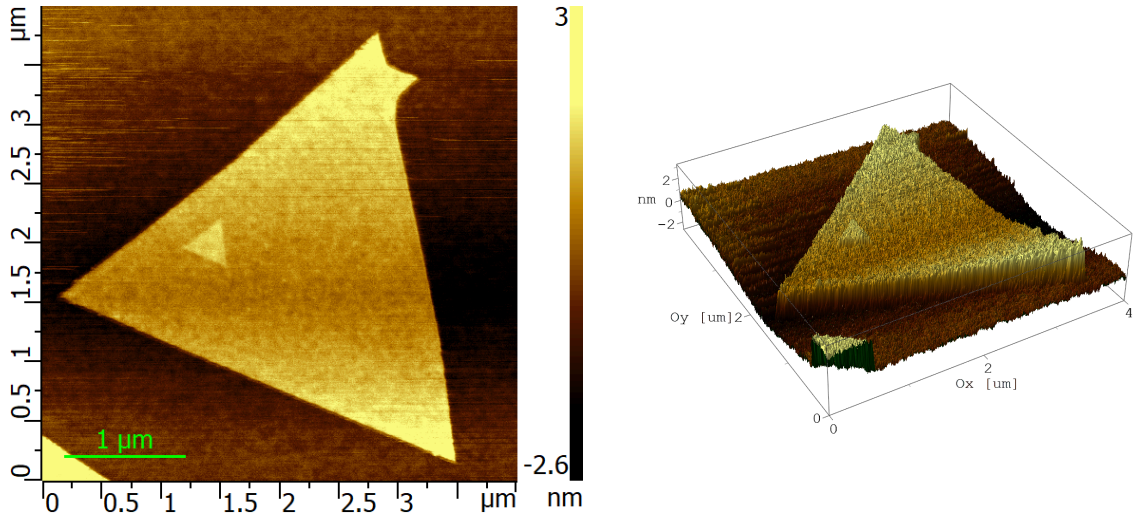

Figure 10. AFM image (left) and 3D AFM image (right) of a CVD grown MoS_2 flake.

In summary, the face-to-face CVD growth successfully produced very thin MoS_2 flakes. The domains were relatively large (tens of microns) and exhibited the expected monolayer Raman and PL signatures. The material's optical responses (Raman peak positions and PL intensity) suggest a low concentration of defects: the PL was quite strong and the exciton peak narrow, implying crystalline, clean monolayers. This is an important achievement because it shows that CVD, a scalable technique, can yield monolayer MoS_2 of a quality approaching that of exfoliated flakes. The main differences observed were the presence of grain boundaries (in areas where domains merged) and some variability in flake size and distribution. Optimizing the seeding and growth conditions could further improve the coverage to eventually get continuous films. Nonetheless, these results demonstrate the core objective of growing very thin MoS_2 via an improved CVD method.

Electrical Test of TiN and Measurement Challenges

Using the mini-probe station described earlier, we first validated its operation with the TiN-coated substrate. In that test, as noted, the four probe tips were placed on the TiN film a

few millimeters apart, effectively contacting four points on a uniform conductor. The I–V measurement produced a straight line through the origin (Ohm's law behavior) with slope corresponding to the sheet resistance of TiN over that probe spacing. The linear I–V and negligible voltage drop at zero current confirmed that the probe tips made good ohmic contact to the TiN and that the measurement circuit had no significant offsets. This gave us confidence that the probe station could be used for real samples.

The next step was intended to be applying this probe station to a MoS_2 device. Our original plan was to use the probe station to measure PL under the low temperature (cryogenic). However, a significant instrumentation challenge prevented this during the project: the optical microscope used on our spectrometer setup could not focus on the sample when the probe station was in place, due to the limited working distance of the objective. As a result, we could not perform these measurements on the CVD MoS_2 monolayers in this thesis work. This outcome is essentially a null result, but it is important to document because it pointed out a critical improvement needed in our setup. We highlight that the inability to probe the monolayers was not due to the material but due to the microscope optics. Acquiring a long-working-distance objective is planned for future experiments so that the monolayer devices can be tested.

Given this limitation, we shifted our focus to extracting as much information as possible from non-electrical characterization. The optical (Raman/PL) and AFM measurements provide a wealth of information about the material's quality and thickness, and these can be correlated with what one would expect for electrical performance (for instance, a monolayer with strong PL and no defects likely has good transport properties, whereas a defective layer might show poor PL and also poor mobility). In the Discussion section, we will reflect on what the optical data imply for electronic quality and the plan for eventual electrical probing.

Co-Localized Multi-Technique Characterization and point measurements of Exfoliated MoS_2 Flakes

To establish a baseline for what a high-quality monolayer MoS_2 looks like across different measurements, we performed an in-depth analysis of the selected exfoliated MoS_2 flakes. This flake was identified via optical microscopy and preliminary spectroscopy as a likely monolayer. We then mapped its Raman, PL, and AFM signals all on the same region. The goal was to see a consistent story: that the flake's optical spectra and physical thickness all indicate a single-layer MoS_2. The surprising result, as we will detail, was that we were able to perform co-localized AFM and Raman, but we could not get the proper PL results. Thus, we decided to perform single point acquisition in different spots of different heights. However, we still wanted to get a full co-localized picture. We performed the technique on the other flake (flake 2) that was also a candidate for monolayer. Interestingly, while Raman and PL indeed showed monolayer characteristics, the AFM did not.

Optical Appearance: Under the microscope, the flake's central region was almost invisible except for a faint bluish tint, consistent with monolayer thickness (few-layer flakes in the same sample showed progressively more visible interference colors). When the 532 nm laser was focused on this flake, a bright green luminescence spot could be seen by the eye through the microscope, already hinting that the flake emits strongly (monolayer-like).

Figure 11. Optical image of flake 1 (left) and flake 2 (right).

AFM Topography Results: After confirming the flakes were optically a few layers thick (by contrast), we performed AFM scans to measure their thickness. The AFM results were very successful for flake 1 and unexpected for flake 2. Flake 1 gave a thickness of a single layer, a bilayer, 7-8 nm, and 10nm. This is a perfect flake to study how Raman/PL differs with the different number of layers.

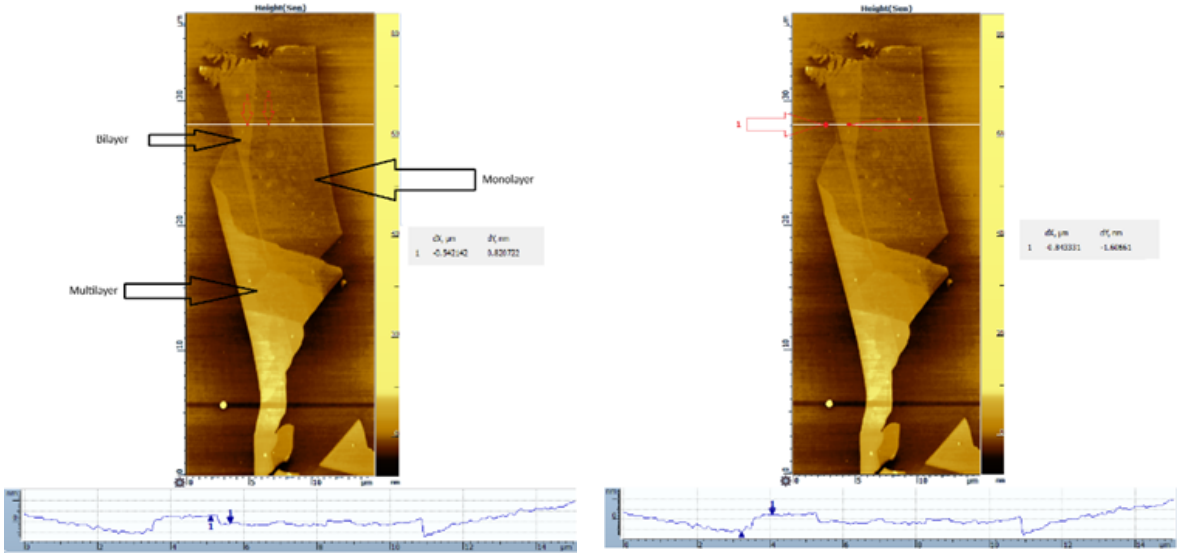

Figure 12. AFM image of monolayer (left) and bilayer (right) regions of Flake 1.

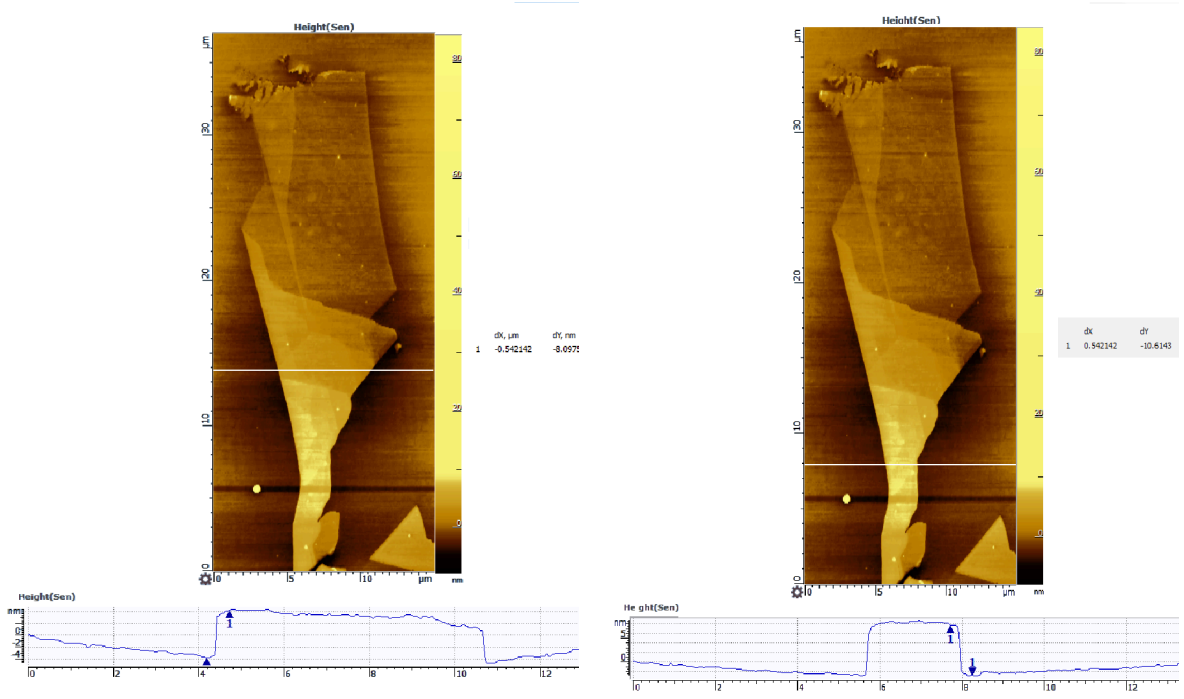

Figure 13. AFM image of 7-8 nm (left) and 10 nm (right) regions of Flake 1.

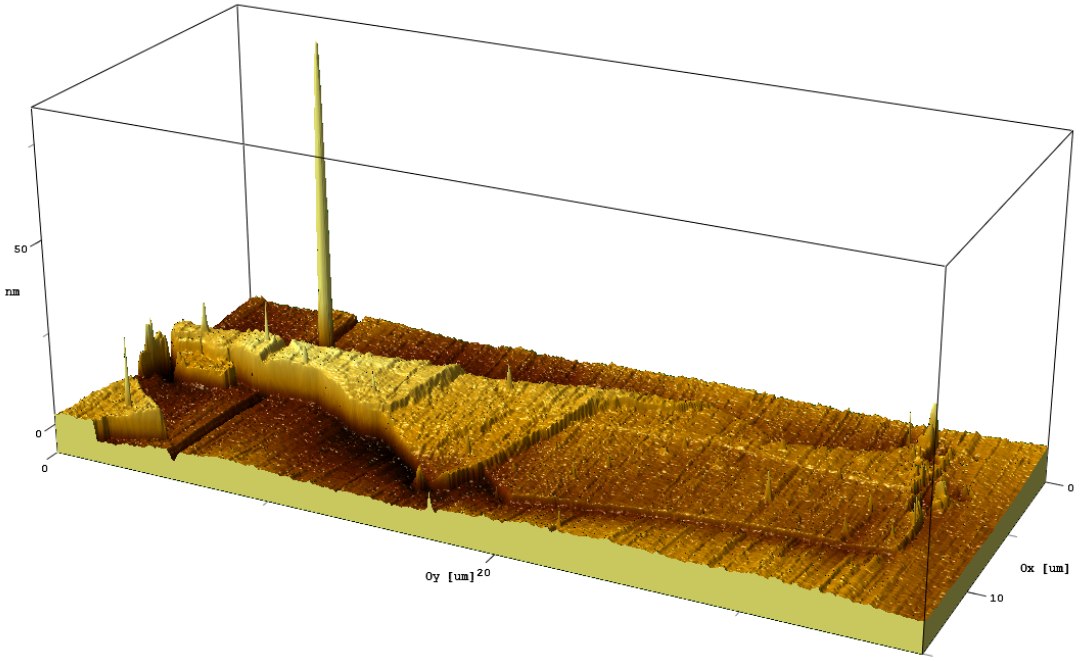

Figure 14. 3D AFM image of Flake 1.

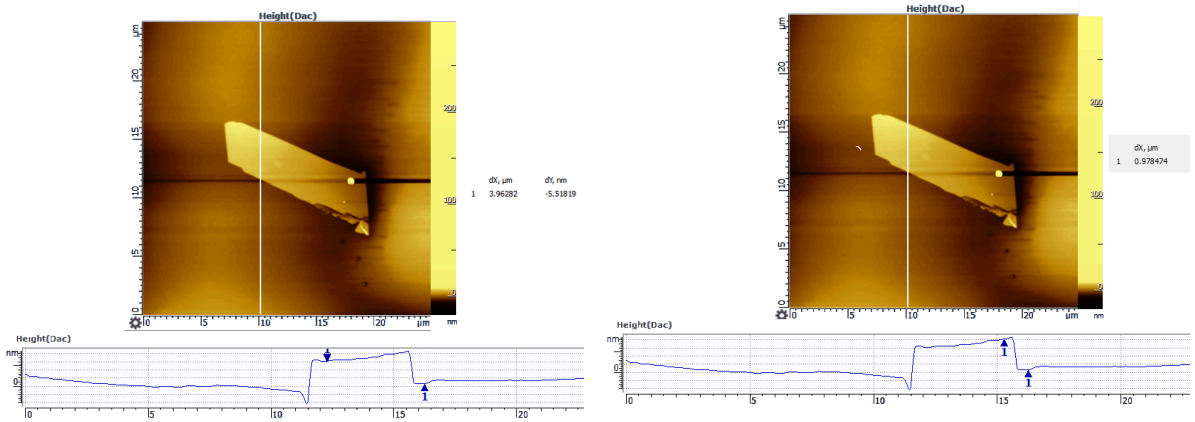

Figure 15. AFM image of Flake 2 with varying thickness of 5.5- 7.6 nm.

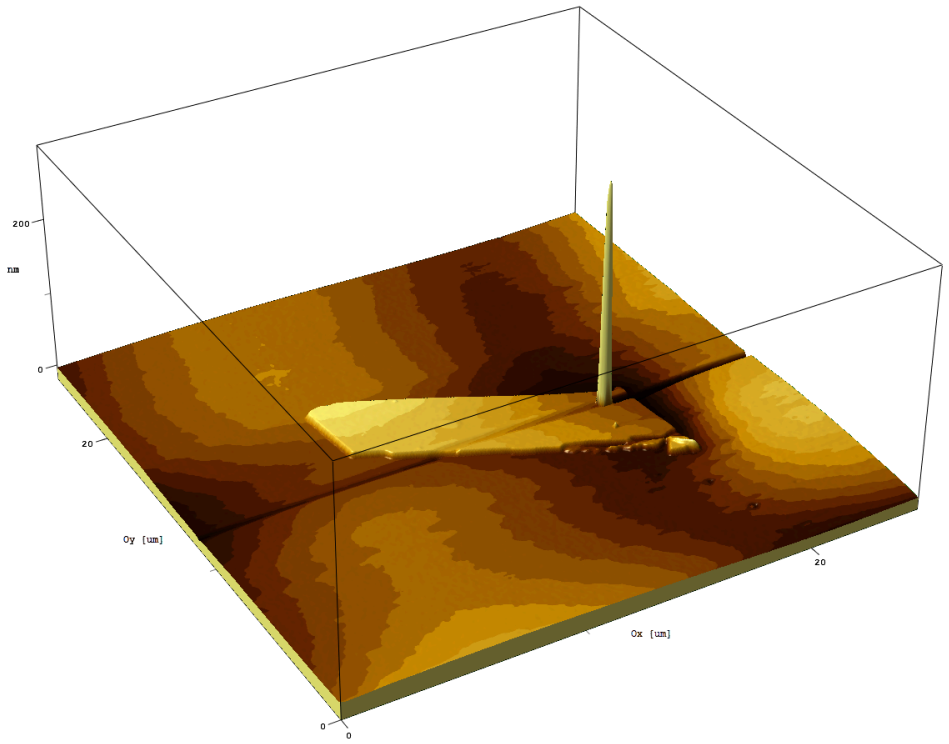

Figure 16. 3D AFM image of Flake 2. (The spike is probably a dust grain)

As shown in the AFM image (Figure 14), the flake appears as a topographic plateau of about 7 nm height above the surrounding substrate. Specifically, line scans across the flake showed a step of approximately 5.5-7.6 nm from the SiO_2 surface to the top of the flake. The flake did not exhibit multiple layer steps or terraces; instead, it was one relatively flat region at ~6-8 nm height. The edges of the flake were somewhat sloped or tapered (likely an artifact of either edge folding or the tip convolution), but the central area clearly sat around 7 nm high. This is orders of magnitude larger than the ~0.7 nm expected for a single MoS_2 monolayer. To put this in perspective, 6-8 nm of MoS_2 would correspond to roughly 10 layers if it were a solid stack (since 1 layer is ~0.65 nm of MoS_2 layer + some van der Waals gap). Yet our optical data showed no signs of multi-layer behavior. The AFM image also did not show any

particles or polymers on top of the flake that could account for 5.5- 7.6 nm of material – it looked smooth.

This presents an apparent contradiction: Raman and PL indicate a monolayer, but AFM indicates something much thicker. We double-checked calibration (the AFM showed the SiO_2 substrate flat and any noise <1 nm, so 5.5- 7.6 nm is a real measurement). We also considered whether the flake could be partially suspended or bubbled. If the flake was not lying flat on the substrate but was instead bridging a tiny gap (perhaps due to trapped air or residue), the AFM would measure the top of the flake relative to the substrate bottom. For example, a monolayer suspended over a ~6 nm tall blister or piece of dust could give such a reading. However, one would expect to see some dome shape if it were a bubble, and our AFM shows a fairly even height across the flake. Another possibility is a transparent residue layer underneath the flake. If some polymer or thick contaminant remained on the substrate and the flake sat on that, the AFM would measure the combined height. Such a residue might be invisible optically (if it's uniform and thin, it might not interfere with optical contrast much, especially if it's something like a thin polymer or an oxidized layer). It is worth noting that we did not intentionally apply any polymer, but tape adhesive might leave some residue. Also, SiO_2 surfaces often have a few monolayers of adsorbed water; however, 5.5- 7.6 nm of adsorbed water is implausible in ambient conditions (typically, a few Ångströms of water layer exists).

We aligned the AFM and optical images to ensure the same flake was being analyzed (there was no mix-up). The co-localization confirmed: the region that Raman/PL maps showed as monolayer corresponds exactly to the region AFM shows as ~5.5- 7.6 nm thick. Thus, it's not that we measured a different area—it's truly the same spot giving conflicting information.

Raman Mapping Results: The co-localized Raman map of the flake 1 (15 μm × 40 μm area) confirmed that with the higher number of layers in the MoS_2, the Raman intensity of ~385 cm^{-1} peak and ~404cm^{-1} increased as well, although slightly higher for ~404cm^{-1} peak (Figure 17).

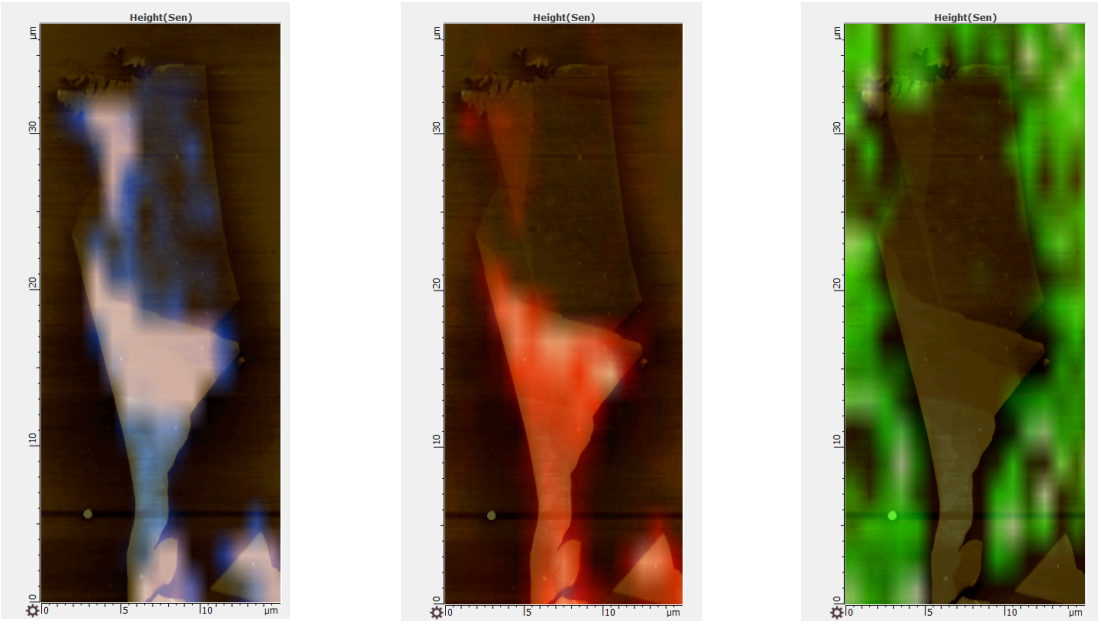

Figure 17. Co-localized Raman spectroscopy map of flake 1. ~385cm^{-1} peak intensity (left). ~404cm^{-1} peak intensity (mid). 520cm^{-1}peak intensity (right).

Figure 18 shows a representative Raman spectrum from the flake's single layer point. At a single layer it has two prominent peaks at approximately 384 cm^{-1} and 400 cm^{-1}. The separation is ~16 cm^{-1}, which is squarely in the monolayer range. Across the single layer region of the flake, this peak positions and spacing were consistent (variations of only ±1 cm^{-1}). The intensities of the Raman peaks were also relatively uniform across the flake's center. No additional peaks (such as disorder-related modes or secondary phase peaks) were observed, suggesting the flake is purely 2H-MoS_2 with low defect density.

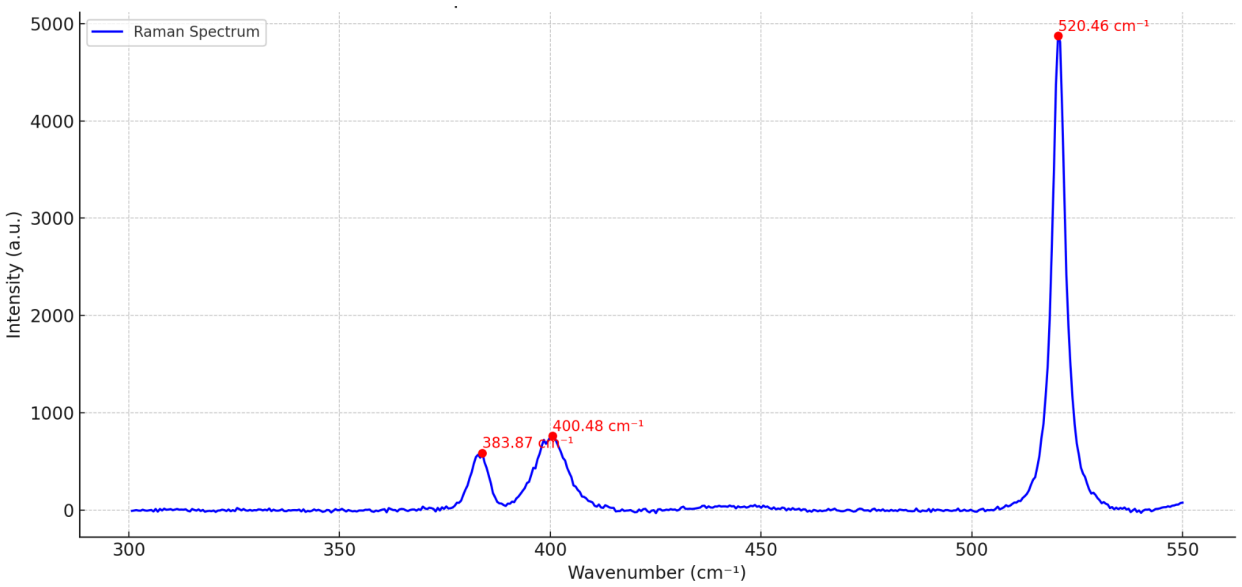

Figure 18. Raman spectrum of the exfoliated MoS_2 flake 1 (532 nm excitation) in a single

layer region. The two main peaks are the E' mode at ~384 cm^{-1} and the A'_1 mode at ~400 cm^{-1}, with a separation of ~16 cm^{-1} confirming monolayer MoS_2. 520 cm^{-1} peak is Si.

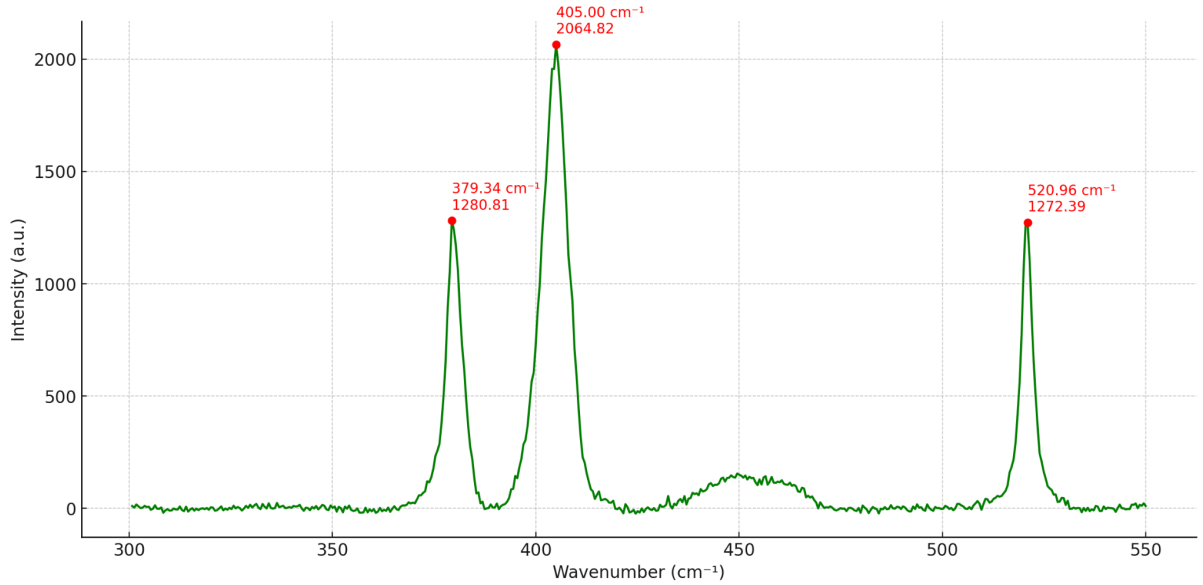

Figure 19. Raman spectrum of the exfoliated MoS_2 flake 1(532 nm excitation) in a multilayer region. The two main peaks are the E' mode at ~379 cm^{-1} and the A'_1 mode at ~405 cm^{-1}, with a separation of ~26 cm^{-1} confirming multilayer MoS_2. 520 cm^{-1} peak is Si.

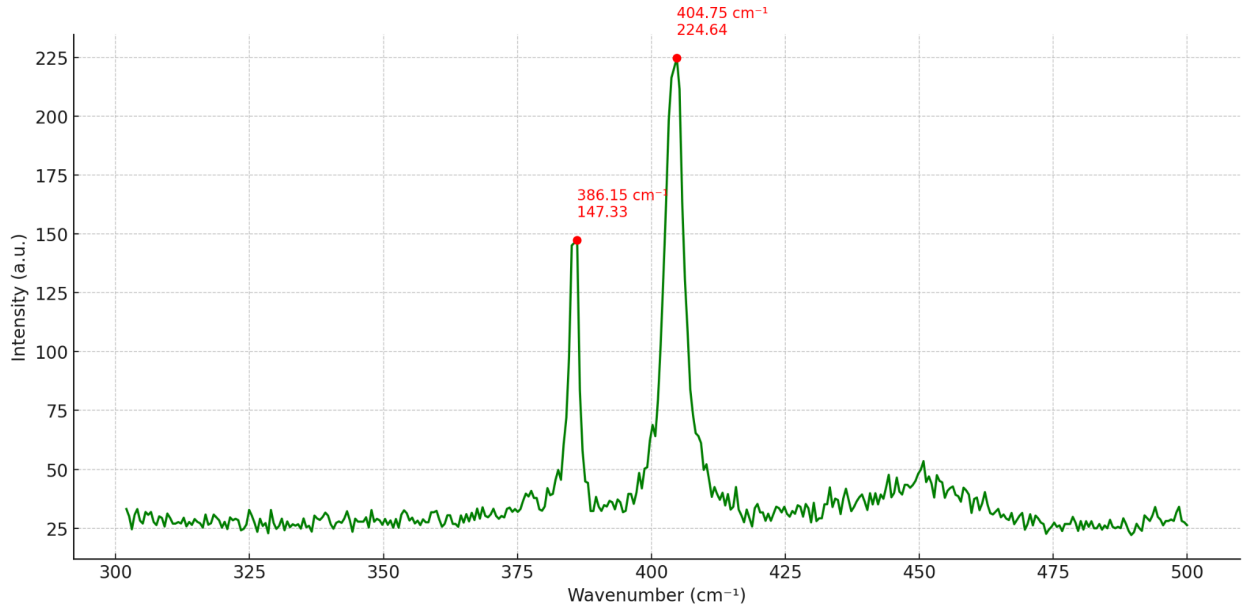

Figure 20. Raman spectrum of the exfoliated MoS_2 flake 2 (532 nm excitation). The two main peaks are the E' mode at ~386 cm^{-1} and the A'_1 mode at ~405 cm^{-1}, with a separation of ~19 cm^{-1} confirming monolayer MoS_2.

Figure 20 supports the idea that optically chosen flakes are indeed showcasing monolayer features.

Photoluminescence Mapping Results: The PL map of the same area showed a strong, uniform photoluminescence emanating from the flake 1 monolayer region. A representative PL spectrum is shown in Figure 18. The flake exhibited a pronounced PL peak at ~1.85 eV (≈674 nm) with a high intensity (on the order of 10^5 counts at peak, given our detection setup). This peak corresponds to the A exciton of monolayer MoS_2. The full-width at half-maximum of the peak was around 55 meV, which is quite narrow for room temperature and indicates good optical quality (sharp PL implies low inhomogeneous broadening from defects or strain). Importantly, there was no secondary PL peak at ~1.3 eV (which would indicate the indirect bandgap emission of bilayer or bulk MoS_2). The absence of any low-energy PL feature and the high intensity of the ~1.85 eV emission confirm that the flake is behaving optically as a monolayer. The PL intensity map was bright across the flake and dropped to nearly zero off the flake, showing a clear contrast between the monolayer area and the substrate. Towards some edges of the flake, the PL did decrease slightly, which could be due to edge nonradiative recombination or possibly the presence of a few-layer-thicker edge (edges can sometimes be multilayer if the flake has thicker sections at its periphery). However, within the central area, the PL was consistently strong. These PL observations, together with the Raman results, gave us high confidence that the flake's region was a monolayer of MoS_2.

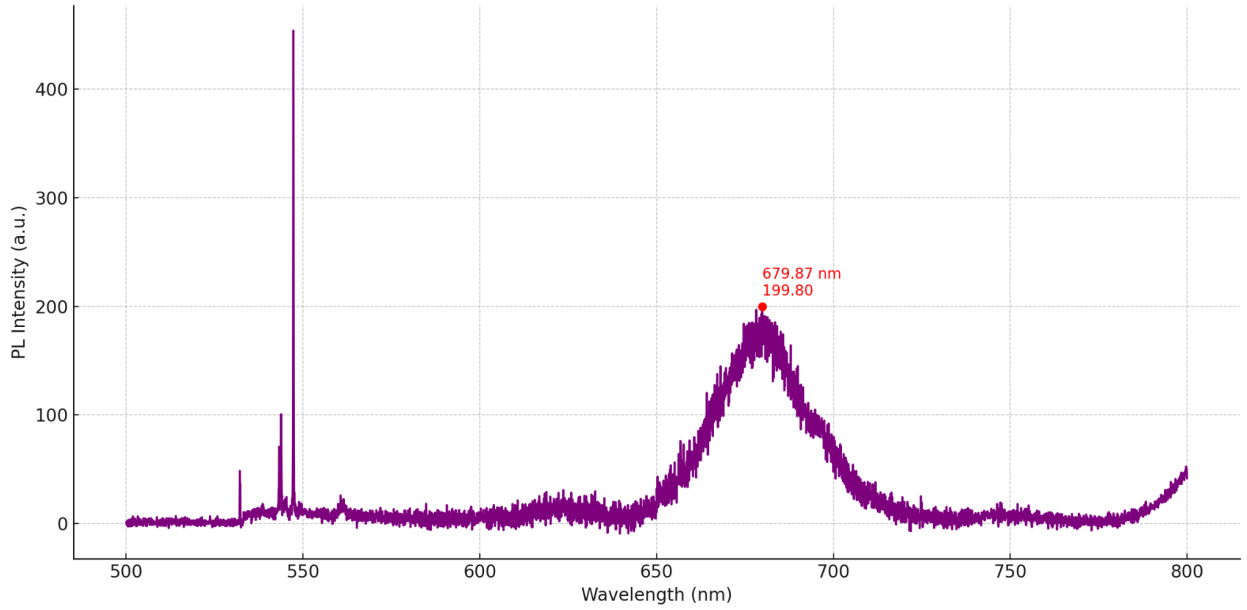

Figure 21. Photoluminescence spectrum of the exfoliated MoS_2 flake 1 at single layer region. A single strong PL peak is seen at ~1.82 eV (680 nm), corresponding to the A exciton of monolayer MoS_2. The high intensity and lack of lower-energy emissions indicate a direct band gap monolayer. The PL peak width (~30 nm) is consistent with a high-quality monolayer with low defect density.

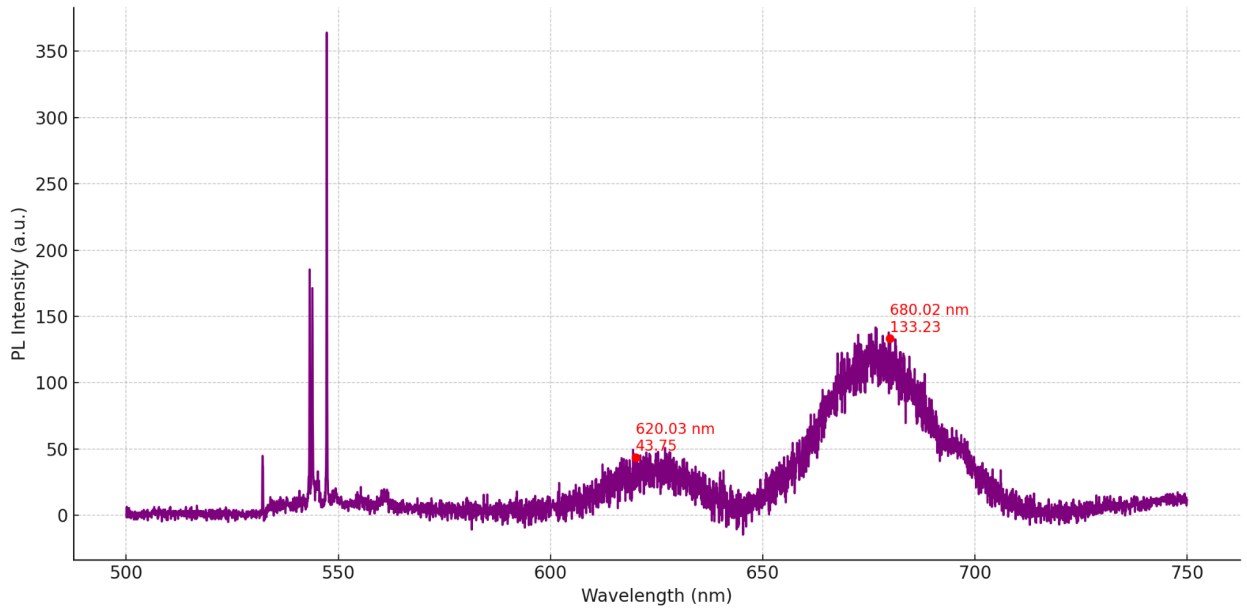

Figure 22. Photoluminescence spectrum of the exfoliated MoS_2 flake 1 at bilayer region. The intensity of the main peak at ~1.82 eV (680 nm) is lower and the "shoulder" is appearing.

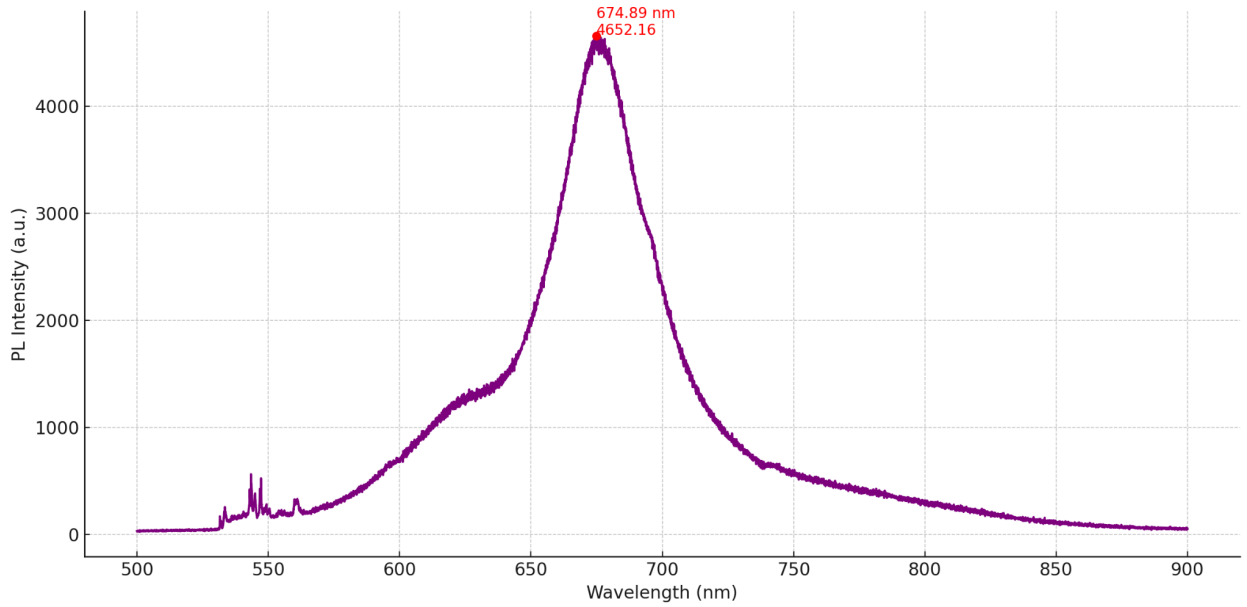

Figure 23. Photoluminescence spectrum of the exfoliated MoS_2 flake 2. Intensity is different due to different settings.

Summary of Observations: the summary of the multi-modal measurements on two exfoliated MoS_2 flakes reveals both consistent and contradictory findings, highlighting the advantages and disadvantages of each method. The core portion of flake 1 displays all the characteristics of a monolayer, according to the perfect agreement between the Raman, PL, and AFM data. AFM thickness of ~0.8 nm, strong PL at ~1.85 eV with narrow FWHM, and Raman peak separation of ~16 cm^{-1} all clearly show a high-quality monolayer. Bilayer, few-layer, and thick (~10 nm) areas are also present in the same flake, which offers a useful

internal control over how Raman and PL vary with layer number. According to these results, flake 1 is a trustworthy standard for characterizing monolayer MoS_2.

Conversely, Flake 2 offers a perplexing contradiction. Peak locations, intensities, and PL spectral shape are all consistent with a direct bandgap monolayer, which is again supported by Raman and PL data. AFM scans, however, show a flat, continuous topography throughout the same area with a thickness of 5.5–7.6 nm. Because of this disparity between optical and physical measurements, meticulous alignment and double-checking were necessary. The co-localized maps attest to the fact that every approach examined the same region. Despite considering a number of theories (such as residue layer, trapped air gap, and tip convolution), no definitive explanation was found. Flake 2 is more difficult to comprehend since it lacks internal height fluctuation, in contrast to flake 1.

I present the data as is for the purposes of this section. I will examine the potential causes of this AFM–optical mismatch in the Discussion section. Interestingly, despite its atypical physical structure, flake 2's Raman and PL measurements remain a second reference point for optically high-quality monolayer MoS_2. These results highlight the value of multi-technique, co-localized analysis in 2D materials research. Using just one method can result in inaccurate results, especially when it comes to monolayer identification. After characterizing both flakes, we proceed to analyze these results, contrast them with our CVD-grown samples, and look more closely into the causes of the thickness anomalies.

Discussion

Comparison of MoS_2 from CVD Growth vs. Exfoliation

The CVD-grown monolayer MoS_2 domains and the mechanically exfoliated monolayer flake both exhibit strong monolayer characteristics in Raman and PL, indicating that, in terms of optical and vibrational properties, they are quite similar. This is a significant finding: it suggests that our face-to-face CVD method can produce monolayers that are nearly as optically high-quality as those from exfoliation (which are often considered the “gold standard” for material quality). For instance, the PL peak of the CVD monolayers (~1.85 eV) was as intense and narrow (on the order of tens of meV FWHM) as that of the exfoliated flake. This implies low defect density and good crystal quality in the CVD material. Raman spectra of both samples showed sharp E' and A'_1 peaks with the expected spacing, and no additional defect modes, again pointing to good crystallinity.

However, there are inherent differences due to the methods of preparation. The exfoliated monolayer originates from a bulk single crystal, so it is essentially a single-crystalline sheet with no grain boundaries. Its lateral size is limited by what can be peeled off – in our case, on the order of 10 μm (though in other attempts, exfoliated flakes tens or even hundreds of microns are possible if one is lucky). The CVD monolayers, in contrast, are grown on a substrate in a non-equilibrium process. Each triangular domain we grow is a single crystal domain of tens of microns, which is impressive and comparable to small exfoliated flakes. But when multiple domains coalesce, they form grain boundaries at the meeting lines. These

grain boundaries are line defects in the film – they could potentially scatter charge carriers or serve as recombination centers for excitons.

Another difference is substrate interactions and unintentional doping: CVD growth occurs on the substrate, so the MoS_2 might pick up some impurities from the growth process or have strain from thermal expansion mismatch on cooling. Exfoliated flakes are placed on the substrate at room temperature, so they might have less built-in strain. At least optically, the CVD and exfoliated monolayers are comparable.

In terms of morphology, the CVD monolayers in our study often had triangular shapes dictated by the crystallographic growth facets (typically, MoS_2 triangles are terminated by Mo-edges or S-edges depending on conditions). The exfoliated flake had an irregular shape (broken jagged edges from the mechanical cleaving). But that is a superficial difference. More importantly, the domain size: achieving a continuous film by CVD would require those triangles to merge without significant gaps or misorientation. One could envision a continuous monolayer film across the substrate. Exfoliation will never give that – it will always be random flakes.

The exfoliated MoS_2 flakes were thoroughly examined using atomic force microscopy (AFM), Raman spectroscopy, and photoluminescence (PL) to cross-validate their layer thickness and material quality. This multi-modal characterization provides a comprehensive understanding of each flake, as each technique probes different aspects of a monolayer. Raman identifies vibrational modes whose frequency difference shifts with layer number, PL reveals the direct bandgap emission unique to monolayers, and AFM directly measures the topographical thickness. By applying all three techniques on the same regions of each flake (co-localized measurements), we ensured consistent identification of monolayer areas and minimized the chance of misinterpreting a flake's true thickness.

Flake 1 exhibited *i*nternally consistent results across AFM, Raman, and PL, conclusively identifying it as a monolayer. AFM measurements of Flake 1's central region showed a thickness of approximately 0.8 nm, which is in line with the expected height of a single MoS_2 layer on SiO_2 (taking into account a nominal monolayer thickness of ~0.65 nm plus a typical interfacial layer). Raman spectroscopy of this flake revealed the characteristic pair of peaks (the in-plane E′ mode and the out-of-plane A'_1 mode) with a separation on the order of 15–20 cm^{-1}, consistent with literature values for monolayer MoS_2. Photoluminescence further confirmed the monolayer nature: Flake 1 showed a single, strong PL peak at around 1.82–1.85 eV (~680 nm) corresponding to the A exciton of monolayer MoS_2, with no low-energy secondary peak (which would have indicated the indirect bandgap emission of a bilayer or thicker material). The PL emission was intense and relatively sharp (narrow full-width at half-maximum), suggesting high optical quality and a low defect density in the flake. Taken together, these observations leave little doubt that the examined region of Flake 1 is indeed a monolayer. Notably, Flake 1 also contained some thicker sections at its periphery (bilayer, few-layer, and ~10 nm multilayer regions were identified elsewhere on the flake in the AFM scans). These served as an internal reference: as the layer number increased, the Raman peaks shifted and the PL intensity diminished, which was consistent

with expected trends. This built-in comparison further bolstered confidence in the assignment of the central region as monolayer. Overall, Flake 1 can be considered a high-quality monolayer benchmark for MoS_2, against which other samples can be evaluated.

In contrast, Flake 2 presented a perplexing discrepancy between the optical and AFM measurements. Raman and PL data from Flake 2 were characteristic of a monolayer: the Raman spectrum showed the expected modes for single-layer MoS_2 (with peak positions similar to Flake 1), and the PL exhibited a dominant direct-bandgap exciton emission (again near ~1.85 eV) with no indication of a bilayer's indirect emission. These optical signatures strongly suggested that the MoS_2 in Flake 2 is structurally a monolayer. However, AFM scans of the very same region (carefully aligned to the area probed optically) told a different story. The AFM measured a thickness of approximately 5.5–7.6 nm across Flake 2, and the topography appeared as a flat, continuous slab of that height relative to the substrate. In other words, AFM indicated a thickness on the order of 8–10 monolayers. This is an order of magnitude thicker than the ~0.8 nm one would expect for a single layer, yet the lack of any Raman/PL features of multilayer MoS_2 implies the material is not actually a multilayer stack in the usual sense. The fact that all three techniques examined the same location (via co-localized mapping and reference markers) means this conflict is genuine and not due to looking at different parts of the sample. Thus, Flake 2 forced a careful reconsideration of how each measurement is interpreted.

Several hypotheses were considered to explain the AFM anomaly in Flake 2 (i.e. why a monolayer optically would exhibit a 5–7 nm thickness profile in AFM):

- **Substrate residue or interfacial layer:** There may be an undetected thin film between the MoS_2 monolayer and the SiO_2 substrate – for example, remnant polymer from the exfoliation process or a layer of adsorbed water. Such residue could prop the flake up above the substrate, increasing the apparent thickness. Indeed, previous studies have found that mechanically exfoliated 2D crystals can have intercalated water layers or other contaminants at the interface, leading to an inflated AFM step height. In Flake 2's case, a ~5 nm thick transparent residue layer (if present) could make a one-atom-thick flake appear ~6 nm tall in AFM, even though the MoS_2 itself is monolayer.

- **Trapped air gap or contaminants:** If the flake did not adhere perfectly to the substrate, there could be microscopic voids or pockets of air trapped underneath. A continuous air gap would also manifest as an increased thickness in AFM since the instrument measures the distance from the substrate to the top of the flake. Similarly, aggregates of airborne contaminants trapped under or on the flake could create a uniform height offset. However, one might expect such voids or particles to cause some irregularity in the topography (e.g. bubbles or bumps), whereas Flake 2's AFM topography was relatively uniform.

- **Measurement artifacts (AFM-related):** It is possible that the AFM measurement itself introduced errors. One known issue is tip convolution – if the AFM tip has a finite radius, it may not fully penetrate into narrow gaps at the flake edges, causing the measured step height to appear larger. Additionally, electrostatic forces between the AFM tip and the sample can sometimes lead to overestimation of height if not properly compensated. In non-contact or tapping mode AFM, electrostatic or van der Waals interactions can effectively lift the tip slightly off the true surface. Such factors can be particularly misleading on 2D materials, which are extremely thin and can be influenced by surface charges.

Despite these plausible explanations, no single definitive cause was identified for Flake 2's behavior. The flake's surface was smooth and did not show obvious signs of a ~5 nm contaminant film (e.g. no distinct layers or patches were visible that could be peeled off). Efforts such as gentle sample heating or repeated scanning (if performed) did not reveal any changes that would point to a removable layer or collapse of an air gap. Thus, the discrepancy remains unresolved: Flake 2 appears to be a monolayer that is somehow effectively "thicker" in AFM. It is likely that a subtle combination of factors – for instance, a very uniform ultra-thin residue or water layer that is hard to detect optically, coupled with slight AFM measurement bias – is responsible. This finding serves as a cautionary example that even with high-precision tools, anomalies can occur if the sample has hidden complexities.

Crucially, the case of Flake 2 underscores the importance of co-localized, multi-technique analysis for accurate layer identification. Had we relied on a single characterization method, we could have easily misidentified the sample. For example, using only AFM data, one would conclude Flake 2 was a multilayer film (~7 nm thick). Conversely, using only Raman and PL, one would be convinced it was a monolayer and might remain completely unaware of the physical thickness anomaly. By comparing and cross-verifying findings from all three techniques on the same region, we obtained a more nuanced understanding: the MoS_2 crystal is monolayer in terms of its lattice and electronic structure, but something extrinsic is affecting its effective thickness. This multi-modal approach thus provided a critical cross-check, revealing an exception that calls for careful interpretation. In general, our results highlight that no single technique is infallible; combining surface topography and spectroscopic signatures is the most reliable way to identify monolayer 2D materials and to avoid false conclusions.

Furthermore, the excellent agreement of techniques in Flake 1 means that such exfoliated monolayer flakes can serve as benchmark references for other samples, particularly those grown by methods like chemical vapor deposition (CVD). Exfoliated Flake 1, being a confirmed high-quality monolayer, establishes baseline values for key indicators: for instance, the Raman mode frequencies and their separation, the PL peak energy and intensity, and the AFM thickness on a given substrate. When evaluating CVD-grown MoS_2 domains, one can compare their Raman and PL responses to that of Flake 1 to judge whether the CVD sample has indeed achieved monolayer status and how its quality compares. In our work,

having Flake 1 as a reference standard was invaluable for interpreting the CVD-grown films in a later stage, as it provided a direct point of comparison for what "true" monolayer signals look like. In summary, the detailed study of these exfoliated flakes not only confirmed their properties but also reinforced broader lessons: multi-technique verification is essential for 2D materials, and high-quality exfoliated monolayers are extremely useful as calibration standards for novel or less well-understood samples.

Instrumentation Challenges and Future Work

Besides materials-related insights, this project shed light on an important instrumentation challenge: the optical alignment in the mini-probe station. As discussed, the short working distance of the microscope objective prevented us from measuring low-temperature PL of MoS_2 samples. This limitation has clear implications for our ongoing and future experiments.

Impact of the Probe Station Limitation: The inability to probe the monolayers electrically means we currently lack direct transport data on our CVD-grown material. All assessments of quality are indirect (from optical signals). While strong PL and sharp Raman spectra suggest good electronic quality, they do not replace actual measurements of carrier mobility, contact resistance, etc. Key questions such as "Do grain boundaries significantly reduce electron mobility?" or "Is there unintentional doping in the CVD MoS_2 that shifts its threshold voltage?" remain unanswered without electrical data. Thus, solving this alignment issue is critical to complete the loop of characterization. It's worth noting that our TiN test verifies the station works in principle; it's the optical access that's the bottleneck. In future iterations, we must ensure our setup accommodates both the physical probes and the optical focus.

Planned Improvements: The straightforward solution is to acquire a long working distance (LWD) objective with high magnification. Such objectives are designed to focus from farther away. We will procure an objective (e.g., 50× or 20× with >20 mm working distance) that can be used in our spectrometer setup. With this, we should be able to perform low-temperature measurements.

Future Electrical Measurements: Once the above improvements are made, the immediate plan is to fabricate simple electrode patterns on the CVD-grown MoS_2 monolayers and measure their electrical characteristics. For instance, we can make a two-terminal device by evaporating metal contacts on opposite ends of a monolayer domain, or a field-effect transistor by adding a gate. We expect, based on the optical quality, that the monolayer will show decent mobility and high on/off ratio. If, for example, we measure a mobility of >10 $cm^2/V \cdot s$ and on/off $>10^6$, that would confirm that our CVD material is device-worthy. If the performance is lower, it may indicate issues like charged impurity scattering (perhaps from residues or substrate effects not seen optically). Additionally, electrical testing could reveal if there are Schottky barrier problems at the metal-MoS_2 contacts that need optimizing.

Bridging electrical and optical data will also unlock new experiments. We could apply a gate voltage and observe changes in PL (as electrons are added, neutral excitons convert to negatively charged trions, altering PL intensity and peak position). This kind of coupled

electro-optical experiment can provide deeper insight into recombination dynamics and doping in the material (Outline.docx).

Finally, addressing the instrumentation will allow us to probe the anomalous flake electrically as well. If that flake is contacted, we could see if it behaves like a monolayer transistor (high on/off) or like a thicker semiconductor (maybe much lower on/off). That might indirectly tell us if it's electronically a monolayer or not.

In summary, the probe station issue, while a setback in this project, clearly defines a to-do item for future work. We have identified the required hardware fix (LWD optics). Implementing that will enable us to fully characterize the monolayers we have grown, correlating optical quality with electronic performance – a necessary step toward applying these materials in real devices.

Conclusion

In conclusion, the multi-modal characterization of exfoliated MoS_2 flakes yielded a robust understanding of their layer composition and highlighted the strengths of a combined analytical approach. Flake 1 was unambiguously identified as a monolayer, confirmed by the convergence of evidence from AFM (expected one-layer thickness), Raman (signature vibrational frequencies of a single layer), and PL (strong direct bandgap emission). This consistency across techniques validates Flake 1 as a genuine monolayer and attests to its high crystalline quality. Flake 2, on the other hand, displayed a surprising inconsistency: it exhibited all the optical hallmarks of a monolayer but an anomalously large AFM thickness (5.5–7.6 nm). This finding serves as a reminder that even in carefully prepared exfoliated samples, unforeseen factors can influence certain measurements.

Overall, the findings demonstrate the critical value of combining Raman spectroscopy, photoluminescence, and AFM for reliable verification of monolayer MoS_2. Each method on its own provides important information, but also has potential pitfalls – and in the case of Flake 2, relying on any single technique could have led to an incorrect conclusion. By using a coordinated, multi-technique approach, we achieved a high degree of confidence in identifying monolayer regions and we were able to detect and scrutinize anomalies when they arose. The observed discrepancy in Flake 2 underscores the need for continued investigation into substrate interactions and measurement nuances: further work is warranted to pinpoint the cause of such AFM/optical mismatches (be it trace contamination, air gaps, or instrument effects) and to develop strategies to mitigate them (for example, substrate cleaning protocols or alternative AFM modes). A better understanding of these issues will improve the accuracy of thickness measurements for 2D materials.

Looking forward, several future work directions are suggested to enhance and build upon this study. First, integrating a long-working-distance objective into the optical characterization setup would enable cryogenic temperature measurements of Raman and PL on these flakes.

This addition would allow the examination of monolayer MoS_2 at low temperatures (where excitonic and defect-related phenomena can be more pronounced) without compromising the ability to focus on the sample in a cryostat or enclosed environment. Such low-temperature optical studies could reveal further insights into the material's electronic and optical properties (for instance, observing narrow linewidths, defect-bound excitons, or phase transitions) and would complement the room-temperature analysis. Second, improvements to the probe station setup are recommended to facilitate direct electrical probing of the flakes. By outfitting the system with micro-fabricated contacts or maneuverable metal probes, it would become possible to perform in situ electrical transport measurements (such as two-probe or four-probe conductivity tests, or field-effect transistor behavior if the flake is gated) on the very same monolayer flakes that have been optically characterized. Combining electrical data with the existing AFM, Raman, and PL information would provide a more holistic understanding of each sample, linking structural and optical quality to electronic performance. These advancements – cryogenic optical capability and integrated electrical probing – will further strengthen the experimental framework for studying MoS_2 and other two-dimensional materials. By implementing these future improvements and continuing to employ a multi-technique strategy, one can achieve an even more **r**igorous characterization of monolayer MoS_2, paving the way for reliable assessment of new materials and the development of high-performance 2D devices.

In conclusion, this thesis has demonstrated the successful synthesis of MoS_2 monolayers and provided a detailed examination of their properties, while also identifying key challenges and outlining steps to address them. The results contribute to the broader effort in the 2D materials field to reliably fabricate and verify monolayer materials. With the planned future work, we will not only solve the specific puzzles encountered (like the thickness anomaly and probe station issue) but also expand the scope to more materials and devices, thereby continuing the advancement of two-dimensional materials science and technology.

References

1. P. Yang, X. Zou, Z. Zhang, M. Hong, J. Shi, S. Chen, J. Shu, L. Zhao, S. Jiang, X. Zhou, Y. Huan, C. Xie, P. Gao, Q. Chen, Q. Zhang, Z. Liu, and Y. Zhang, "Batch production of 6-inch uniform monolayer molybdenum disulfide catalyzed by sodium in glass," *Nat. Commun.*, vol. 9, no. 1, Art. no. 979, Mar. 2018, doi: 10.1038/s41467-018-03388-5.

2. S. Z. Butler *et al.*, "Progress, Challenges, and Opportunities in Two-Dimensional Materials Beyond Graphene," ACS Nano, vol. 7, no. 4, pp. 2898–2926, 2013.

3. H. Rostami and R. Asgari, "Spin and valley transport in monolayers of MoS_2," *J. Appl. Phys.*, vol. 115, no. 13, p. 133703, Apr. 2014, doi: 10.1063/1.4870040.

4. A. Splendiani *et al.*, "Emerging Photoluminescence in Monolayer MoS_2," Nano Letters, vol. 10, no. 4, pp. 1271–1275, 2010.

5. D. Dumcenco, H. Kobayashi, Z. Liu, Y.-S. Huang, and K. Suenaga, "Large-area MoS_2 grown using H_2S as the sulphur source," *2D Matter.*, vol. 2, no. 4, p. 044005, Nov. 2015, doi: 10.1088/2053-1583/2/4/044005.

6. Y. J. Liu, L. Z. Hao, W. Gao, Y. M. Liu, G. X. Li, Q. Z. Xue, W. Y. Guo, L. Q. Yu, Z. P. Wu, X. H. Liu, H. Z. Zeng, and J. Zhu, "Growth and humidity-dependent electrical properties of bulk-like MoS_2 thin films on Si," *RSC Advances*, vol. 5, no. 91, pp. 74329–74335, 2015. https://doi.org/10.1039/C5RA11454C

7. Liu, J., Fang, M., Yang, EH. et al. Reduction in thermal conductivity of monolayer MoS2 by large mechanical strains for efficient thermal management. Sci Rep 15, 1976 (2025). https://doi.org/10.1038/s41598-024-85060-1

8. H. S. Nalwa, "A review of molybdenum disulfide (MoS_2) based photodetectors: from ultra-broadband, self-powered to flexible devices," *RSC Advances*, vol. 10, no. 51, pp. 30529–30602, 2020. https://doi.org/10.1039/D0RA03183F

9. X. Li and H. Zhu, "Two-dimensional MoS_2: Properties, preparation, and applications," *J. Materiomics*, vol. 1, no. 1, pp. 33–44, Mar. 2015. https://doi.org/10.1016/j.jmat.2015.03.003

10. Edinburgh Instruments, "High-Resolution Raman & PL Imaging of MoS_2," *Edinburgh Instruments*, Jan. 16, 2025. https://www.edinst.com/resource/high-resolution-raman-pl-imaging-of-mos2/

11. Instec, "How to Choose a Heating and Cooling Stage," *Instec*, https://instec.com/portal/article/index/id/30/cid/10.html.

12. T. Korn, S. Heydrich, M. Hirmer, J. Schmutzler, and C. Schüller, "Low-temperature photocarrier dynamics in monolayer MoS_2," *Applied Physics Letters*, vol. 99, no. 10, p. 102109, Sep. 2011. [Online]. Available: https://doi.org/10.1063/1.3636402

13. J. W. Christopher, B. B. Goldberg, and A. K. Swan, “Long tailed trions in monolayer MoS_2: Temperature dependent asymmetry and resulting red-shift of trion photoluminescence spectra,” *Sci. Rep.*, vol. 7, no. 1, p. 14062, Oct. 2017. [Online]. Available: https://doi.org/10.1038/s41598-017-14378-w

14. S. A. F. Rashid, A. A. Aziz, S. R. Majid, and M. A. Mahdi, “Influence of temperature on the electrical properties of TiN thin films deposited by RF magnetron sputtering,” *RSC Adv.*, vol. 5, no. 88, pp. 72083–72091, 2015. https://doi.org/10.1039/C5RA11454C

15. D. P. Khatua, A. Singh, S. Gurung, and J. Jayabalan, "Excitation density dependent carrier dynamics in a monolayer MoS_2: Exciton dissociation, formation and bottlenecking," *Micro and Nanostructures*, vol. 165, p. 207205, 2022, doi: 10.1016/j.micrna.2022.207205.

16. H. Zeng *et al.*, “Valley Polarization in MoS_2 Monolayers by Optical Excitation,” Nature Nanotechnology, vol. 7, pp. 490–493, 2012.

17. Y.-H. Lee *et al.*, “Synthesis of Large-Area MoS_2 Atomic Layers with Chemical Vapor Deposition,” Advanced Materials, vol. 24, no. 17, pp. 2320–2325, 2012.

18. D. Dumcenco *et al.*, “Large-Area MoS_2 Grown Using H_2S as the Sulphur Source,” 2D Materials, vol. 2, no. 4, 044005, 2015.
19. Y. Zhang *et al.*, “Raman Spectra of Monolayer and Few-Layer MoS_2,” Physical Review B, vol. 85, 115317, 2012.

20. K. F. Mak *et al.*, “Atomically Thin MoS_2: A New Direct-Gap Semiconductor,” Physical Review Letters, vol. 105, 136805, 2010.

21. A. Kuc, N. Zibouche, and T. Heine, “Influence of quantum confinement on the electronic structure of the transition metal sulfide TS_2,” *Physical Review B*, vol. 83, no. 24, p. 245213, Jun. 2011.https://doi.org/10.1103/PhysRevB.83.245213